Bioorthogonal labeling tools to study pathogenic intracellular bacteria

Bakkum, T.

Chapter 4

Ultrastructural Imaging of *Salmonella*-Host Interactions Using Super-Resolution Correlative Light-Electron Microscopy of Bioorthogonal Pathogens

Published part of this chapter as part of:

1) Daphne M. van Elsland*****, Sílvia Pujals*****, Thomas Bakkum*****, Erik Bos, Nikolaos Oikonomeas-Koppasis, Ilana Berlin, Jacques Neefjes, Annemarie H. Meijer, Abraham J. Koster, Lorenzo Albertazzi and Sander I. van Kasteren. *ChemBioChem*, **2018**; 19(16): 1766-1770 *(*Authors contributed equally).*

2) Teodora Andriana*****, Thomas Bakkum*****, Daphne M. van Elsland, Erik Bos, Abraham J. Koster, Lorenzo Albertazzi, Sander I. van Kasteren and Sílvia Pujals. *Methods in Cell Biology: Correlative Light and Electron Microscopy IV*, **2021**; Volume 162, Chapter 13: 303-33 *(*Authors contributed equally).*

Abstract

The imaging of intracellular pathogens inside host cells is complicated by the low resolution and sensitivity of fluorescence microscopy and by the lack of ultrastructural information to visualize the pathogens. This chapter describes a new method to visualize these pathogens during infection that circumvents these problems. Using a metabolic labeling approach to bioorthogonally label the intracellular pathogen *Salmonella typhimurium*, in combination with fluorophores that are compatible with Stochastic Optical Reconstruction Microscopy (STORM), and placing this in a Correlative Light-Electron Microscopy (CLEM) workflow, the pathogen can be imaged within its host cell context with a resolution of 20 nm. This STORM-CLEM approach thus presents a new approach to understand these pathogens during infection.

4.1 Introduction

The rise of antibiotic resistance is one of the major threats to global health. One class of pathogens proving particularly troublesome in this regard is that of the intracellular bacteria. These thwart immune detection by residing and replicating inside host-cell phagosomes.[1] Through secretion of factors that manipulate phagosomal maturation, they ensure their intracellular survival, despite an extensive arsenal of defense mechanisms deployed by the mammalian host.[2] It is, therefore, of utmost importance to understand bacterium-host interactions at the cellular and molecular levels. Bioorthogonal chemistry has proven to be a major breakthrough technique to study such host-pathogen interactions. Through hijacking the biosynthetic machinery of the cell wall with biorthogonal analogues of D-alanine[3–5] or trehalose[6–8], intracellular pathogens have been visualized selectively within host-cell phagosomes. Bioorthogonal Non-Canonical Amino acid Tagging (BONCAT[9]) – the incorporation of bioorthogonal amino acids into a target cell proteome – has also proven valuable in this context, for example, to image bacterial protein synthesis or retrieve pathogenic proteins secreted into the host cytosol by *Yersinia enterocolitica*[10], *Salmonella enterica*[11–13], *Escherichia coli*[14], and *Mycobacterium smegmatis*.[15] However, these labeling approaches either require the mutant tRNA/tRNA synthetase pair specific for the bioorthogonal analogue of methionine, phenylalanine, or norleucine analogues to be introduced into the pathogen to achieve incorporation of the desired groups or suffer from low sensitivity.[16] This has limited their use to bacterial strains for which these techniques are available.

In an effort to image the subcellular location of bacteria in host phagocytes, an approach was recently developed that allowed visualization of bacteria within the ultrastructural context of the host cells, by using Correlative Light-Electron Microscopy (CLEM).[17–19] After sectioning frozen cell samples down to a thickness of 75 nm followed by an on-section copper-catalyzed Huisgen cycloaddition (ccHc) reaction[20,21], intracellular BONCAT-labeled *E. coli* were visualized by confocal microscopy. Subsequent Transmission Electron Microscopy (TEM) of the same section allowed the placement of the fluorescent signal within the ultrastructural context of the phagocytic immune cell (phagocyte). If this approach could be extended to pathogenic species, it would provide a powerful tool to study the interaction of host phagocytes with intracellular pathogens. However, for the approach to be of use for unmodified strains, two major constraints relating to both BONCAT and CLEM have to be overcome. The first is the reliance on mutant tRNA/tRNA synthetases for the incorporation of the bioorthogonal amino acids,

compounded by the low overall signal in BONCAT-CLEM (stemming from the thinness of the samples). It was hypothesized that metabolic hijacking approaches reported for *E. coli* auxotrophic strains[22] would need to be extended and optimized to allow sufficient label incorporation with non-auxotrophic bacterial species, thus ensuring their detection by CLEM. The second limitation is related to the CLEM imaging itself: whereas the resolution of the electron micrograph is of the order of 1 nm, that of fluorescence microscopy is limited by the Abbe diffraction limit of half the photon wavelength ($\lambda \approx 250$ nm)[23], resulting in a resolution gap between the two techniques.

Over the last few years, super-resolution imaging techniques have flourished[24], breaking Abbe's law of limiting resolution[25] and allowing for resolution on the nanoscale. Recently, the combination of fluorescent protein super-resolution imaging was combined with CLEM, and this allowed a tenfold improvement in the fluorescence resolution of fluorescent proteins.[26,27] By lowering OsO_4 concentrations during post-fixing and optimizing resin embedding, fluorophore quenching could be partially prevented. This sample preparation technique was reported with both Photoactivated Localization Microscopy (PALM)[26,28,29] and Stimulated Emission Depletion (STED) microscopy in combination with TEM[30–32] and Scanning Electron Microscopy (SEM).[27,33,34] Of the various super-resolution imaging techniques, stochastic optical resolution microscopy (STORM) offers higher spatial resolution and sensitivity[35–38] at the cost of longer acquisition times. Although this is a drawback for *in vivo* imaging, it presents no problem upon imaging fixed sections. The other limitation of STORM is the need to observe close to the glass surface owing to total internal reflection fluorescence illumination. The thinness of the cryo-sections (75 nm) makes the two approaches very compatible. The two-step nature of bioorthogonal ligations also simplifies the STORM-CLEM workflow, because the fluorophore is introduced after the biological time course and sample preparation. The choice of fluorophore can therefore be made independently of the requirements of the biological experiment. The limited availability of dyes for STORM is thus circumvented.[39] The combination of BONCAT-CLEM methodology with super-resolution microscopy could aid in overcoming some of the hurdles related to pathogen BONCAT-CLEM: the sensitivity and suboptimal resolution of confocal fluorescence microscopy. STORM brings the resolution of the fluorescent signals in closer alignment with TEM and improves sensitivity of detection, allowing imaging of genetically unmodified pathogenic bacteria by BONCAT-STORM-CLEM.

One pathogen that would benefit from lifecycle studies using STORM-CLEM is *Salmonella enterica* serovar Typhimurium (*Stm*). This is a Gram-negative facultative intracellular pathogen that ensures its intracellular survival by secreting various effector proteins after uptake.[40] These modulate the maturation of the phagosome in which the bacterium resides to yield a parasitic vacuole suitable for its survival and replication.[41–44] Van Elsland[45] previously reported the successful application of STORM-CLEM for the imaging of *Stm* (**Figure 1**). However, further optimization and validation of bioorthogonal amino acid incorporation is needed to improve the technique and facilitate its translation to other pathogens.

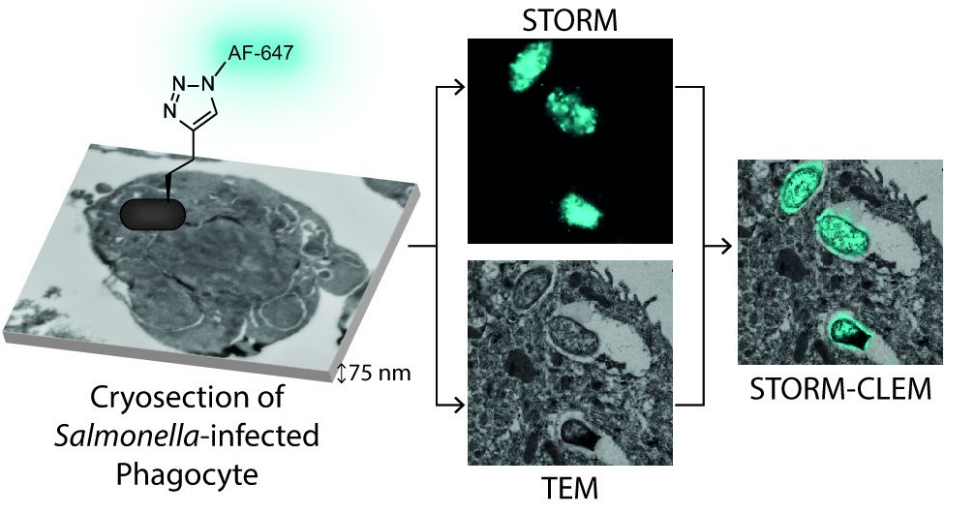

Figure 1. Graphical summary of the BONCAT-STORM-CLEM technique for studying intracellular pathogenic bacteria such as *Salmonella enterica*.

4.2 Results and Discussion

4.2.1 Optimization of bioorthogonal label incorporation in *Stm*

Incorporation of bioorthogonal amino acid analogues was first assessed to allow for optimal ccHc detection of the bacterial proteome while minimizing the effect on bacterial viability and infectivity. Azidohomoalanine (Aha; an azide-analogue of methionine (Met)) was previously used to bioorthogonally label Met-auxotrophic *E. coli* and visualize these bacteria inside bone marrow-derived dendritic cells (BMDCs[46]) using CLEM.[18] In order to find out if non-auxotrophic *Stm* would incorporate Aha into its proteome in detectable amounts, an in-gel fluorescence assay was used (**Figure S1**), using the previously described experimental conditions[18] in which a fluorophore (Alexa Fluor 647; AF647) is attached to the bioorthogonal group through ccHc. Detectable incorporation was observed after a 30 min pulse with Aha (0.04-4 mM) and increases with longer incubation times (60-120 min). These observations were confirmed by flow cytometry, which provides a more accurate representation of the total label incorporation per bacterium. In order to remove any bacteria-unrelated particles from the flow cytometric measurements, the bacteria were gated on size (**Figure S2A**) and shape (**Figure S2B**), and completely non-fluorescent were removed with a cleanup gate (**Figure S2C**). Aha incorporation follows a clear trend, increasing with higher concentrations and longer incubation times (**Figure 2A**, **Figure S3A**) but decreasing again after 30 min at 4 mM or 60 min at lower concentrations. Even after 30 min, close to 100% of bacteria contained sufficient Aha to be detected, no matter which concentration was used (**Figure 2C**). Aha labeling of a DsRed-expressing strain of *Stm*[47] revealed that DsRed fluorescence is slightly reduced with increasing concentrations of Aha (**Figure 2B**, **Figure S3B**). This implies that incorporation of this non-canonical amino acid has a negligible effect on protein function but should simultaneously serve as a warning against excessive label concentrations. *Stm* growth rates remain virtually unaffected up to 30 min incubation with Aha for all of the conditions tested (**Figure S3C**), implying minimal interference with bacterial viability.

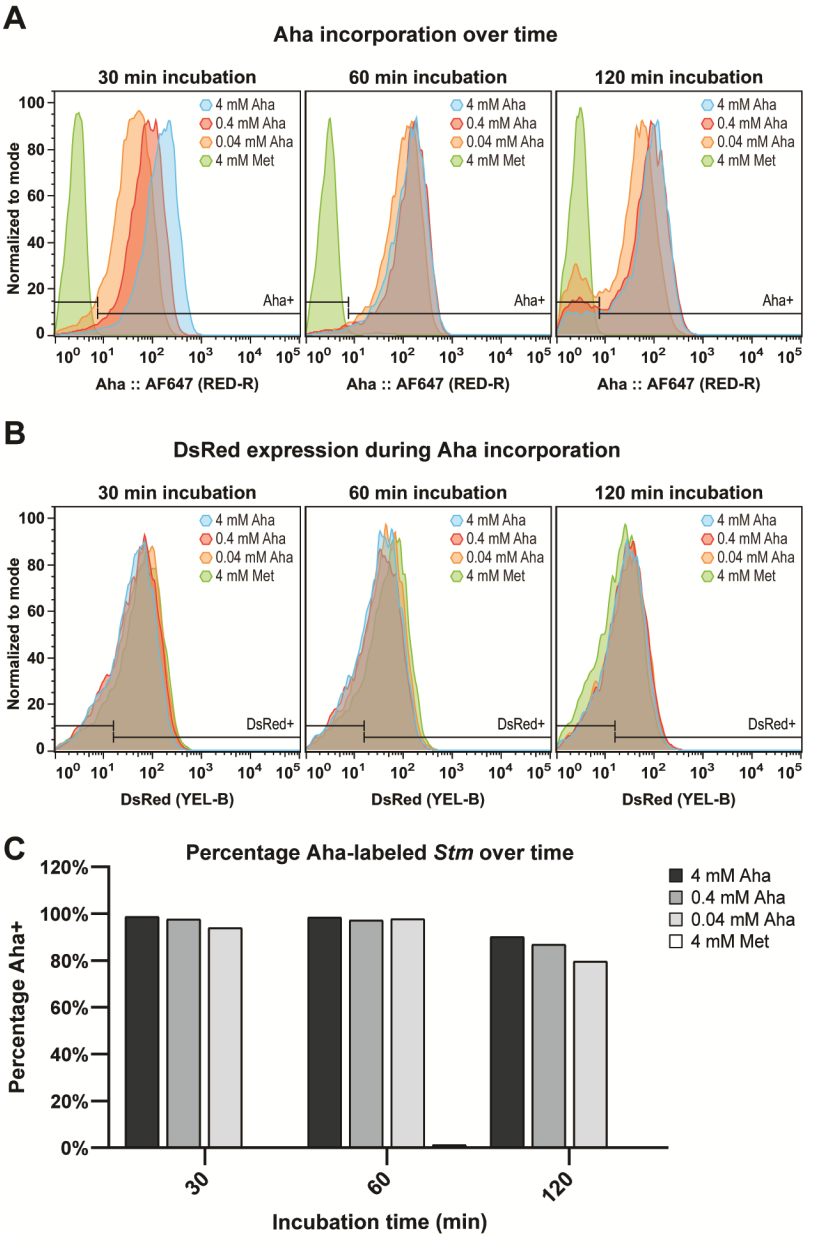

Figure 2. Optimization of Aha incorporation in *Stm* by flow cytometric analysis. DsRed-expressing *Stm* were incubated with increasing concentrations of Aha or 4 mM Met (control) in SelenoMet medium for up to 120 min, then ccHc-reacted with AF647-alkyne for detection by flow cytometry. (**A**) Aha incorporation over time is shown as the flow cytometric distributions of the conjugated AF647. (**B**) The effect of Aha incorporation on the DsRed fluorescent protein is shown as the flow cytometric distributions of DsRed. (**C**) The percentage Aha-labeled *Stm* (Aha+) over time is shown, based on the fluorescence intensity of the reacted AF647 and the threshold set for unlabeled *Stm* (4 mM Met).

Since previous studies revealed that an azide-containing label results in a suboptimal fluorescent signal – due to non-specific reactions of the alkyne-containing fluorophore[48] – the inverse approach was attempted as well. Therefore, incorporation of homopropargylglycine (Hpg; an alkyne analogue of Met) into the proteome was assessed as well using the in-gel fluorescence assay (**Figure S4**). Detectable incorporation was again observed after a 30 min pulse with Hpg (0.04-4 mM) and increases with longer incubation times (1-2 hours). Flow cytometry confirmed a similar trend for Hpg incorporation, increasing with higher concentration and longer incubation times (**Figure 3A**, **Figure S5A**) but plateauing after 30 min at 4 mM or around 60 min at lower concentrations. After 30 min incubation with 4 or 0.4 mM Hpg, nearly all bacteria contained sufficient Hpg to be detected (**Figure 3C**). DsRed fluorescence was virtually unaffected by incorporation of Hpg up to a concentration of 0.4 mM (**Figure 3B**, **Figure S5B**). *Stm* growth rates remain virtually unaffected up to 30 min of incubation with Hpg for all of the conditions tested (**Figure S5C**). Notably, even after a 120 min pulse with Hpg, the growth rates of these Hpg-labeled *Stm* in fresh LB medium recovered to >85% after 120 min for all Hpg concentrations (**Figure S7C**), implying that the observed (minor) growth-inhibiting effect is reversible. Label retention of Hpg-*Stm* during bacterial division ('outgrowth') was also followed by in-gel fluorescence (**Figure S6**) and flow cytometry (**Figure 4A**, **Figure S7A**), following a 120 min pulse with Hpg and a subsequent medium exchange with fresh LB. Nearly all bacteria retained sufficient Hpg to be detected after 120 min of outgrowth (≈2-6 divisions[49]) for all Hpg concentrations (**Figure 4C**). On the basis of these observations, balancing the signal intensity, percentage of Hpg-labeled *Stm* and the impact on growth and DsRed fluorescence, the optimal conditions were chosen as a 30 min pulse with 0.4 mM Hpg.

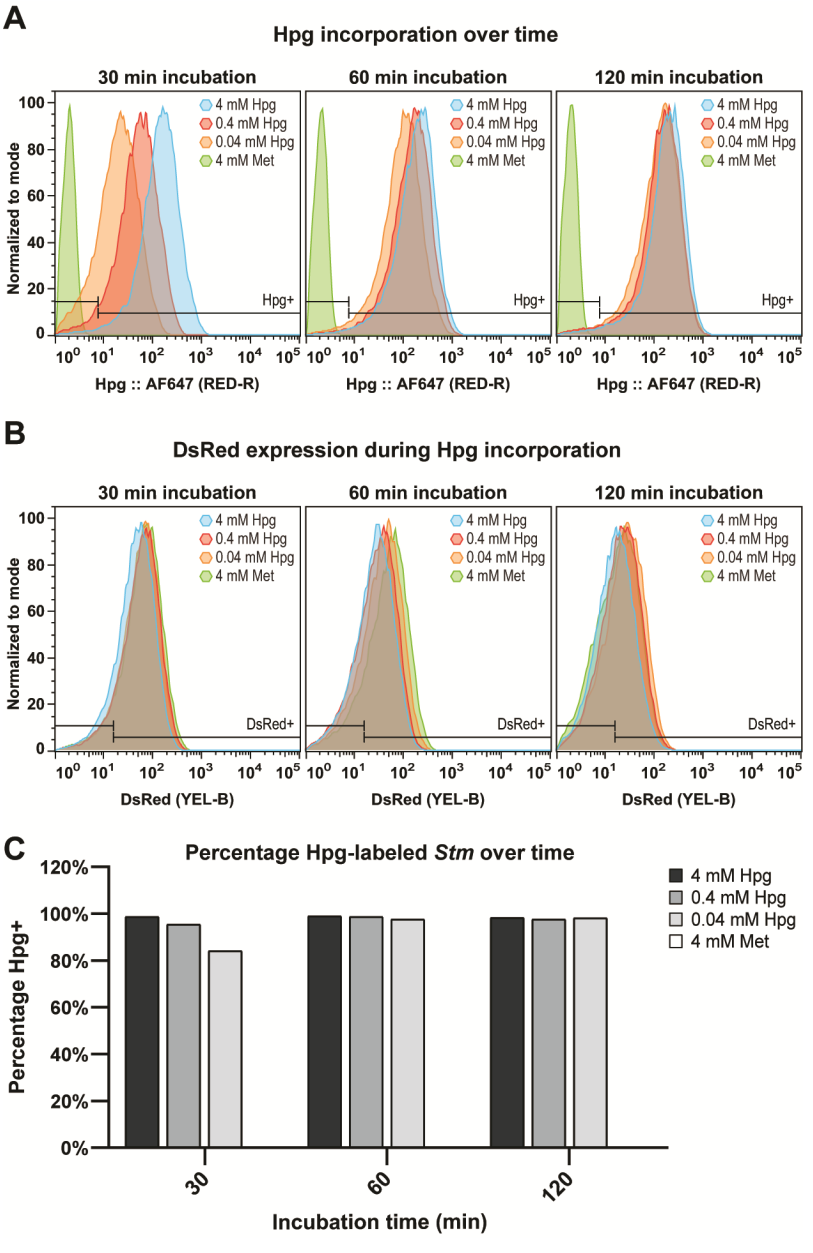

Figure 3. Optimization of Hpg incorporation in *Stm* by flow cytometric analysis. DsRed-expressing *Stm* were incubated with increasing concentrations of Hpg or 4 mM Met (control) in SelenoMet medium for up to 120 min, then ccHc-reacted with AF647-azide for detection by flow cytometry. (**A**) Hpg incorporation over time is shown as the flow cytometric distributions of the conjugated AF647. (**B**) The effect of Hpg incorporation on the DsRed fluorescent protein is shown as the flow cytometric distributions of DsRed. (**C**) The percentage Hpg-labeled *Stm* (Hpg+) over time is shown, based on the fluorescence intensity of the reacted AF647 and the threshold set for unlabeled *Stm* (4 mM Met).

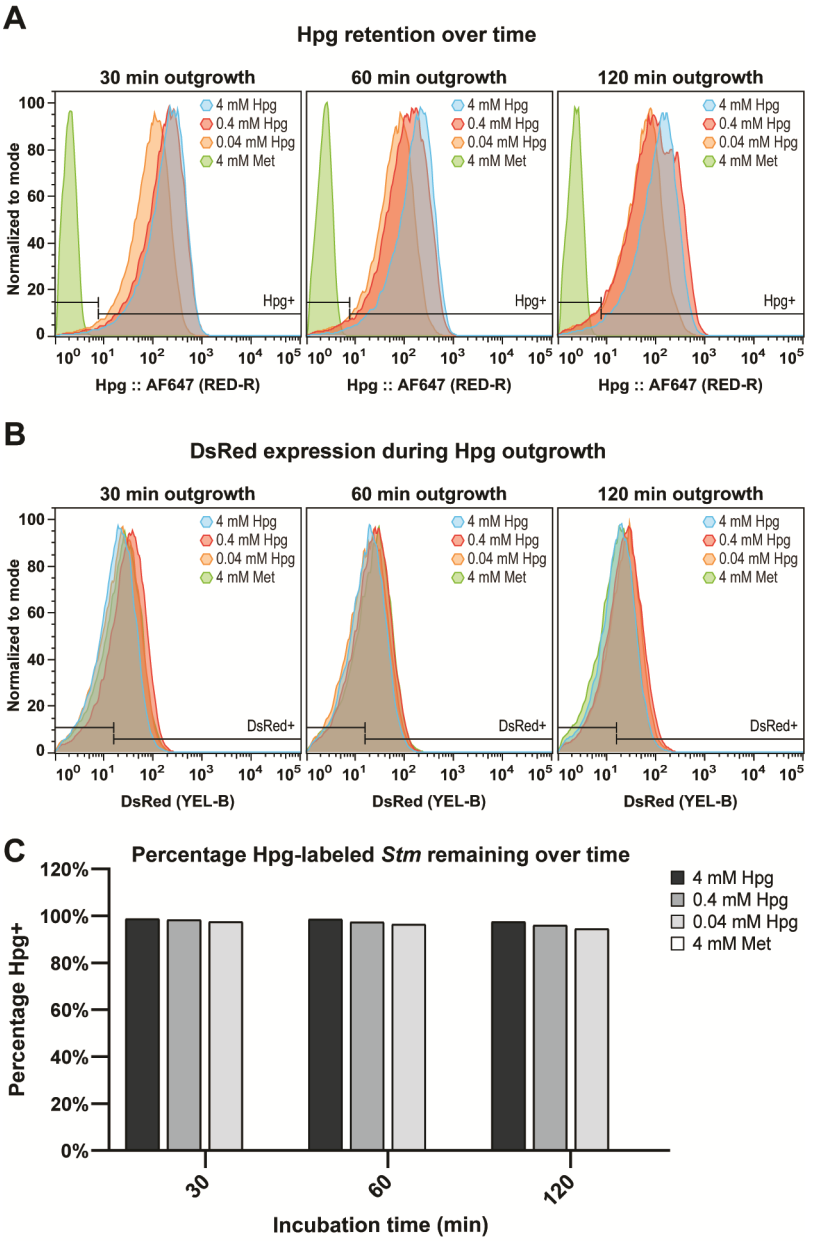

Figure 4. Label retention and growth recovery of Hpg-labeled *Stm* by flow cytometric analysis. DsRed-expressing *Stm* were incubated with increasing concentrations of Hpg or 4 mM Met (control) in SelenoMet medium for 120 min, washed with PBS and resuspended in fresh LB medium and incubated again for up to 120 min, then ccHc-reacted with AF647-azide for detection by flow cytometry. (**A**) Hpg retention over time (outgrowth) is shown as the flow cytometric distributions of the conjugated AF647. (**B**) The effect of Hpg outgrowth on the DsRed fluorescent protein is shown as the flow cytometric distributions of DsRed. (**C**) The percentage Hpg-labeled *Stm* (Hpg+) remaining over time is shown, based on the fluorescence intensity of the reacted AF647 and the threshold set for unlabeled *Stm* (4 mM Met).

Alternatively, D-propargylglycine (alkDala; an alkyne-analogue of D-alanine) could be used to metabolically label the cell wall of *Stm*. If successful, this could additionally allow simultaneous labeling of the cell wall with alkDala and the proteome with Aha. To achieve this, two sequential ccHc reactions with compatible fluorophores (e.g., AF647-azide and AF488-alkyne) are required with intermediate washing steps to remove all excess of the first fluorophore before adding the second. Indeed, incubating *Stm* with 5 mM alkDala for 30 min or longer resulted in a detectable fluorescent signal, measured by flow cytometry (**Figure 5A**, **Figure S8/S9**). Incubating Stm with 5 mM alkDala and 4 mM Aha simultaneously for 30 min or longer resulted in successful dual labeling (**Figure 5C**, **Figure S8/S9**). However, since incubation with alkDala for up to 120 min resulted in less than 60% labeled bacteria (**Figure S8A**), Hpg was used for all subsequent experiments.

To determine whether infectivity was affected for the Hpg-labelled *Stm*, dendritic cells (DC2.4 cell line) were infected for 45 min with the aforementioned DsRed-expressing *Stm*, incubated with either Hpg or Met as a control. Uptake of the bacteria and their subsequent intracellular division were assessed with flow cytometry, measuring the entire *Stm*-containing DCs at different time points. DCs were gated on size, shape and DsRed to select for *Stm*-containing cells (**Figure S10**). By quantifying both the DsRed and bioorthogonal signals over time, bacterial cell divisions and label loss could be calculated simultaneously. Hpg modification did not affect the infectivity of *Stm*, judged by the mean fluorescence intensity (MFI) of DsRed per DC as a proxy of the average number of intracellular *Stm* (**Figure 6A**, **Figure S11A**). Furthermore, the change in DsRed expression over time was the same for both Met- and Hpg-grown *Stm*, indicating no detectable impact of Hpg on intracellular survival and proliferation. Fluorophore ligation of the Hpg-*Stm* within DCs showed only negligible reduction in fluorescent signal per cell over time (**Figure 6B**, **Figure S11B**), confirming previous findings that terminal alkynes are stable to the phagolysosomal pathway.[48] Corresponding *in vitro* controls show a steady dilution of Hpg over time, when the bacteria are able to proliferate freely in label-free medium (**Figure 6C**).

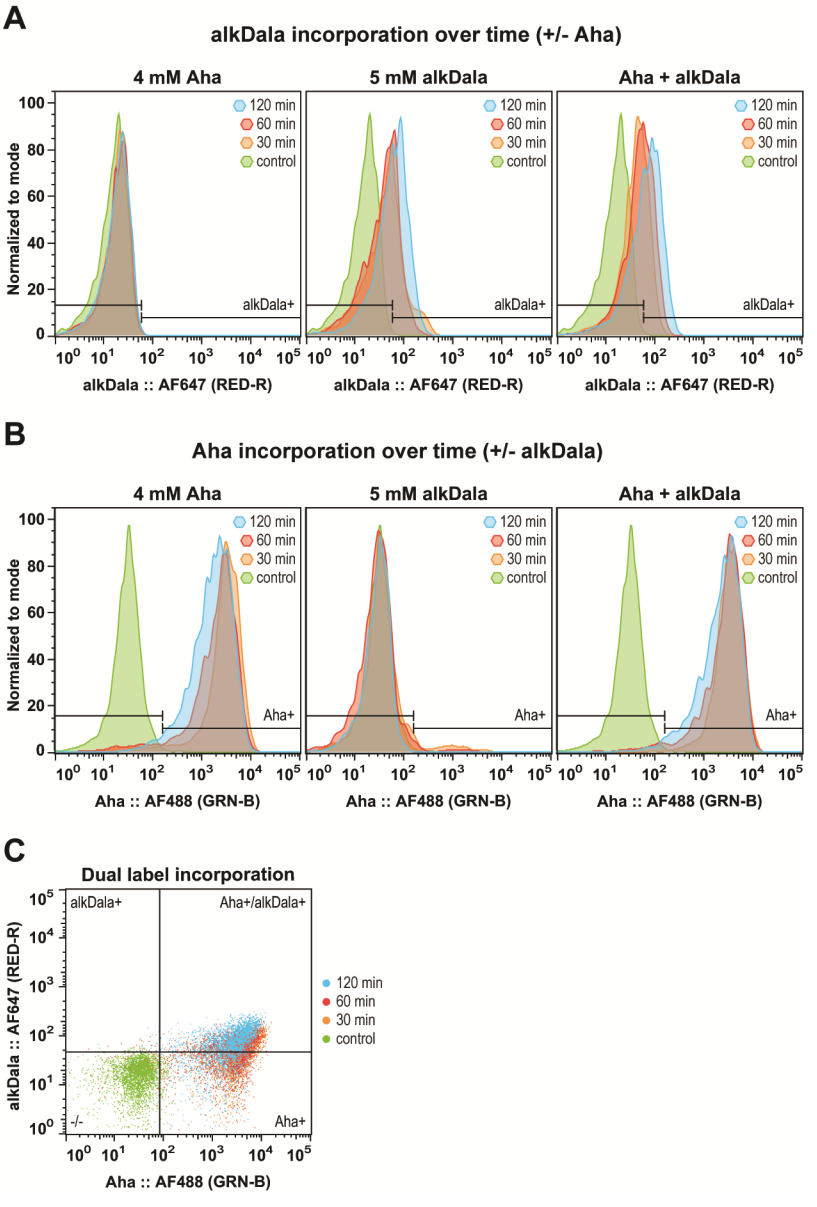

Figure 5. Optimization of alkDala labeling and Aha/alkDala dual labeling of *Stm* by flow cytometric analysis. *Stm* were incubated with 4 mM Aha, 4 mM Met + 5 mM alkDala or 4 mM Aha + 5 mM alkDala in SelenoMet medium for up to 120 min, then ccHc-reacted with AF647-azide (alkDala) and AF488-alkyne (Aha) for detection by flow cytometry. (**A**) alkDala incorporation over time is shown as the flow cytometric distributions of the conjugated AF647. (**B**) Aha incorporation over time is shown as the flow cytometric distributions of the conjugated AF488. (**C**) Dual label incorporation over time is shown as 2-dimensional dot plots of the conjugated AF647 (alkDala) vs. the conjugated AF488 (Aha).

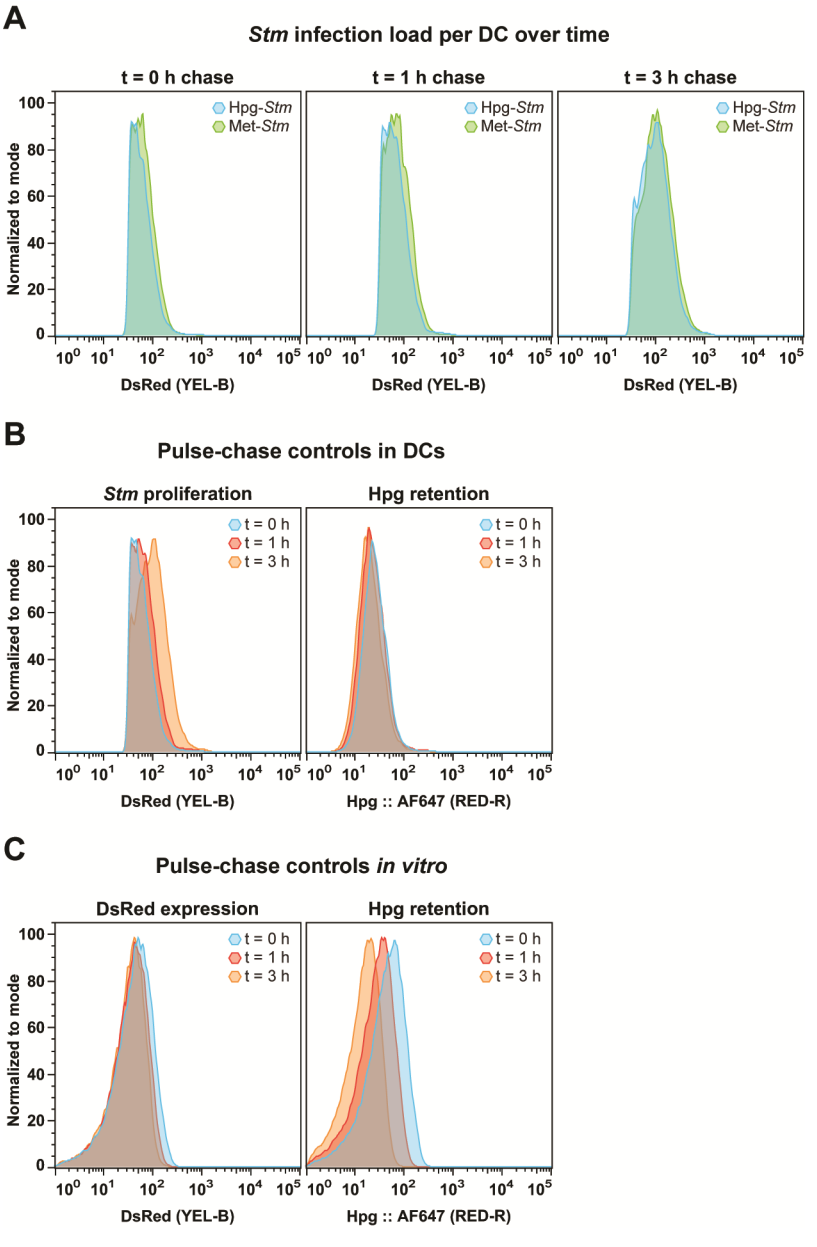

Figure 6. Infection controls, bioorthogonal label retention and *Stm* proliferation in DC2.4 cells. DsRed-expressing *Stm* were first incubated with 0.4 mM Hpg (Hpg-*Stm*) or 4 mM Met (Met-*Stm*) for 30 min in SelenoMet, then washed to remove excess Hpg and added to DCs at an MOI of 50 for 45 min (pulse). *Stm*-infected BDMCs were then washed to remove non-internalized *Stm* and incubated for an additional 0, 1 or 3 hours (chase), followed by ccHc-reaction with AF647-azide for detection by flow cytometry. (**A**) The *Stm* infection load was compared between Hpg-*Stm* and Met-*Stm* over time, based on the DsRed intensity per DC. (**B**) Intracellular *Stm* proliferation and Hpg retention were followed over time in DCs. (**C**) Corresponding *in vitro* DsRed expression and Hpg retention of *Stm* were simultaneously followed over time as controls.

4.2.2 The application of STORM-CLEM to visualize intracellular *Stm* in BMDCs

In order to validate the use of STORM for visualizing Hpg-labeled *Stm* in thin sections that can be used for CLEM, a mixture of labeled and unlabeled *Stm* is required to detect single bacteria without the signals overflowing. To achieve this, Hpg- and Met-grown *Stm* were mixed in various ratios and subsequently fixed for analysis. Flow cytometric analysis revealed that Hpg-labeled bacteria could still be detected at a labeled:unlabeled ratio of 1:25 (**Figure S12**). The detection limit of STORM was then assessed by imaging thin sections of *Stm* grown in the presence of decreasing concentrations of Hpg. Samples were cryo-sectioned, ccHc-ligated with AF647-azide, and imaged by using standard catalase, glucose and glucose oxidase-containing buffer (GLOX) or other oxygen-consuming buffers, such as the OxEA buffer[50] supplemented with 30% glycerol to decrease drift during STORM image acquisition. The acquired STORM images of *Stm* sections labeled with 0.4 or 4 mM Hpg revealed clear bacteria-sized regions (230-400 nm × 180-280 nm, **Figure 7A/B**). *Stm* grown in the presence of 0.04 mM Hpg could be detected, but the signal was too low to allow full reconstruction of the bacteria (**Figure 7C**).

To achieve STORM-CLEM imaging of intracellular *Stm* in BMDCs, Hpg-labeled *Stm* (0.4 mM Hpg for 30 min) were added to a culture of freshly isolated BMDCs at an MOI of 50 and co-incubated for 45 min. After washing away the non-internalized bacteria, the infected cells were processed for cryo-sectioning according to the Tokuyasu method.[18] In short, cells were fixed for 24h in freshly prepared 2% PFA in 0.1M phosphate buffer, embedded in 12% gelatin, cut in cubes of approx. 0.5 mm^3 and sucrose-infiltrated O/N at 4°C. Ultrathin cryo-sections were prepared using a cryo-ultramicrotome and a cryo-immuno diamond knife, transferred to Formvar/carbon-coated titanium TEM grids and thawed in a closed environment to protect from water condensation (suspected to be a major cause of sample deformation and folding). The thawed sections were first incubated on 2% gelatin, then washed with PBS containing 15 mM glycine (to quench any remaining aldehyde residues) and subjected to ccHc-reaction with AF647-azide. Finally, the sections were washed again and the nuclei were counter-stained with DAPI to provide markers for correlation (matching the fluorescence image to the electron micrograph). The fluorescently labeled sections were first imaged with low-resolution confocal fluorescence microscopy (FM) to locate areas of interest and to record the position of the nuclei. Next, the fluorescently labeled *Stm* were imaged by STORM to obtain the corresponding super-resolution fluorescence images. Finally, the sections were post-stained with uranyl acetate (to provide contrast) and imaged by TEM. The resulting images were stepwise correlated to obtain the final

STORM-CLEM image (a projection of the multi-modal dataset). The entire STORM-CLEM protocol is summarized in **Figure 8** and the corresponding workflow and timeline are shown in **Figure 9**.

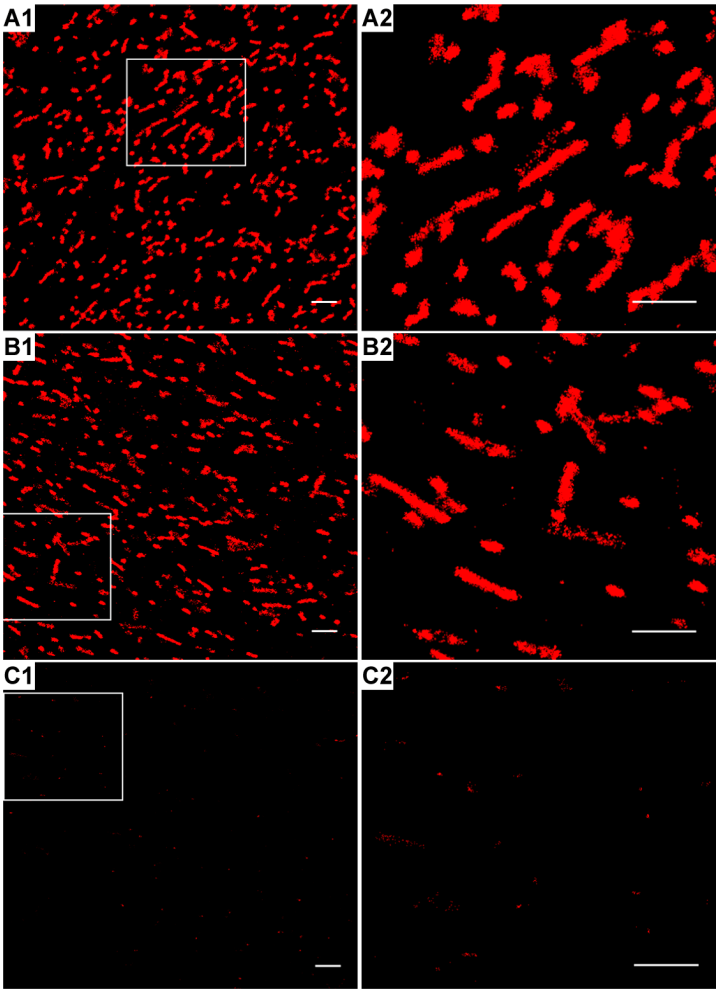

Figure 7. CLEM-compatible ultrathin (75 nm) sections of Hpg-labeled *Stm*, grown in presence of decreasing concentrations of Hpg, mixed in a ratio of 1:25 with unlabeled *Stm*, grown in presence of 4 mM Met. *Stm* were grown in the presence of (**A**) 4 mM Hpg, (**B**) 0.4 mM Hpg or (**C**) 0.04 mM Hpg. The second column (A2-C2) shows zoom-ins of the first column (A1-C1). All scale bars represent 2 µm.

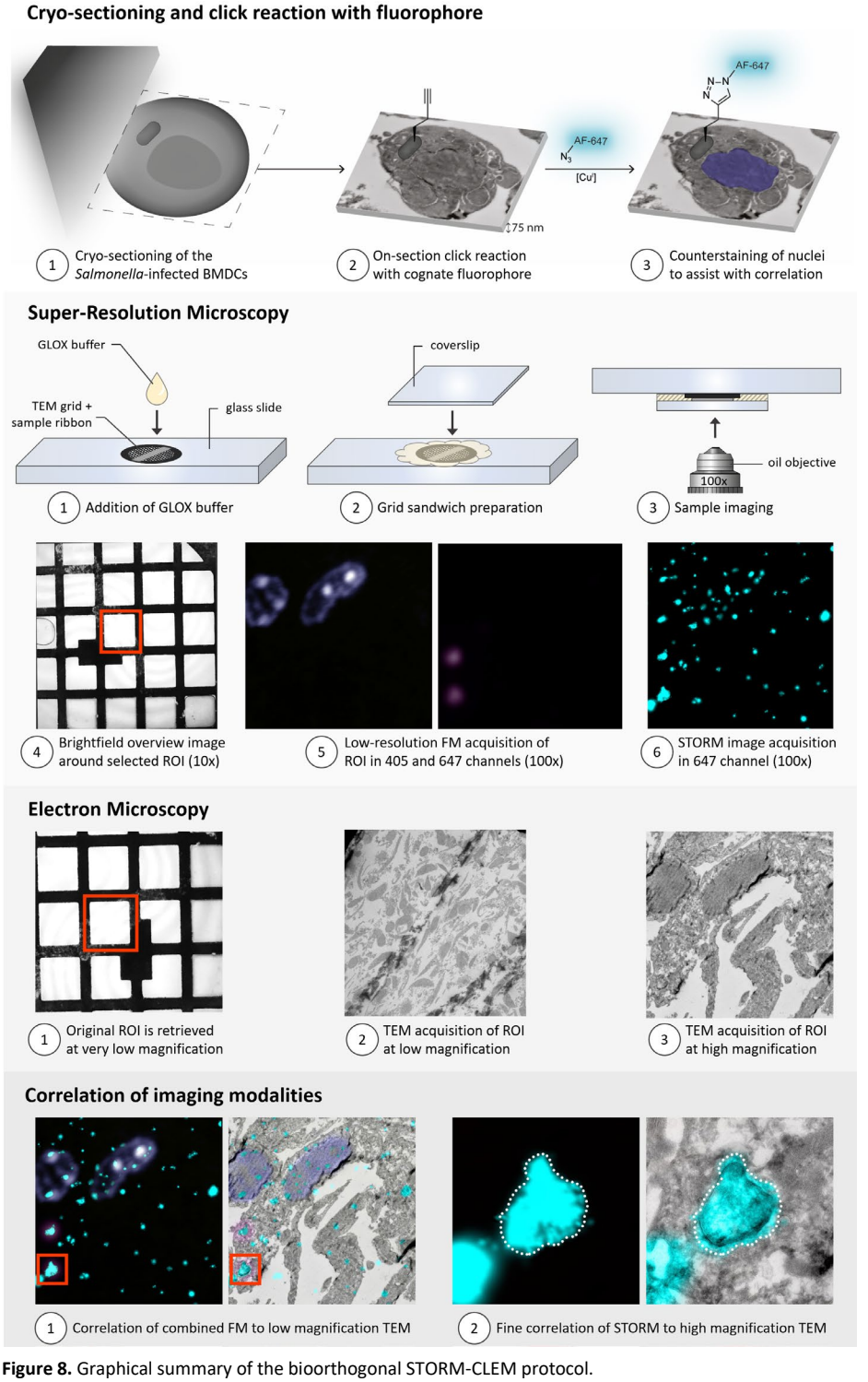

Figure 8. Graphical summary of the bioorthogonal STORM-CLEM protocol.

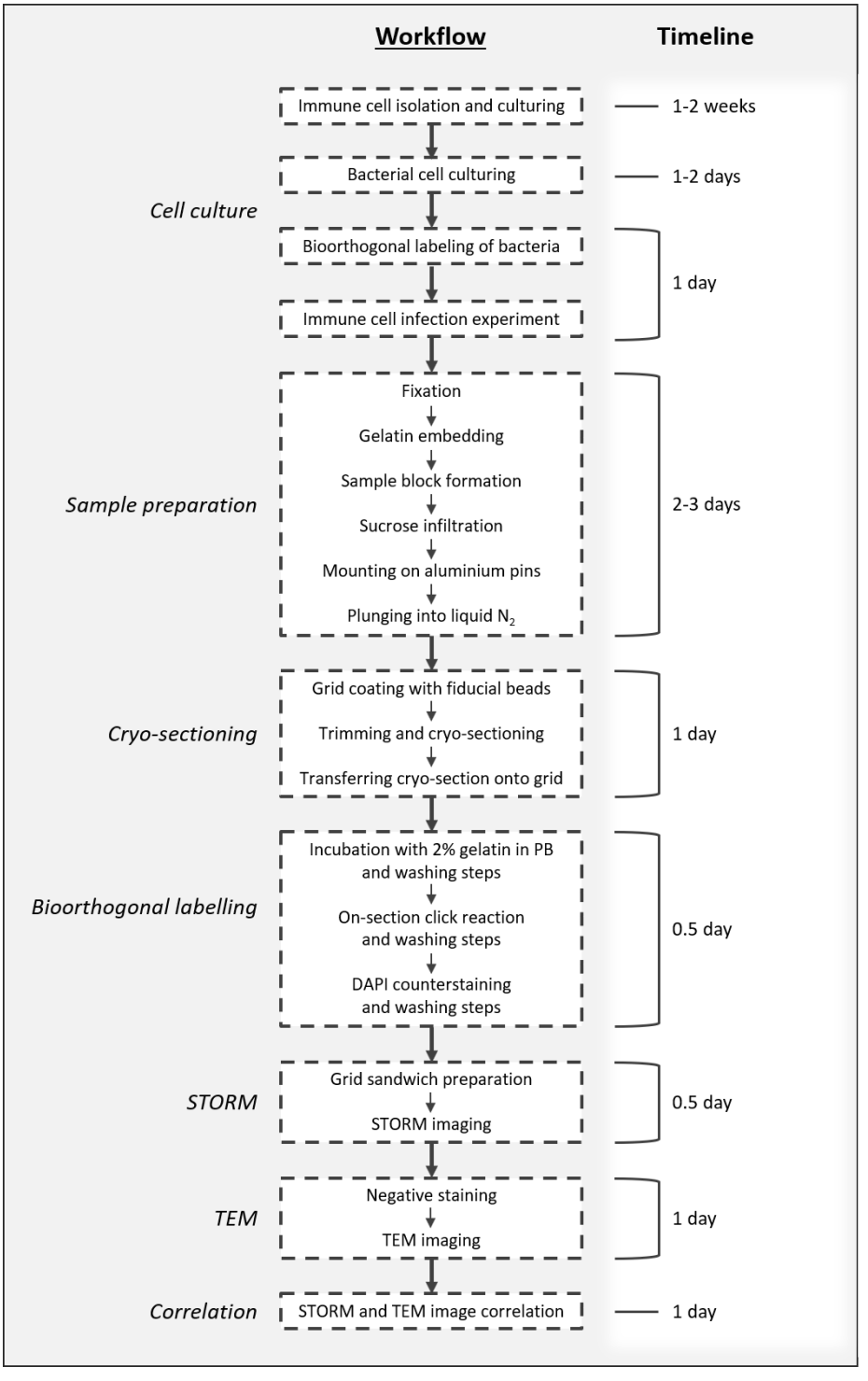

Figure 9. Workflow and timeline of the bioorthogonal STORM-CLEM protocol.

STORM was able to reconstruct the intracellular *Stm* to a high degree, which could then be fitted cleanly onto the bacterial ultrastructure of the TEM image. The sensitivity of STORM allows for the detection of bacterial components that are below the detection limit of low-resolution FM. The observed spatial resolution of STORM is at least tenfold better than the optimal resolution that could be obtained with confocal microscopy (20 nm vs. ~250 nm). Whereas STORM is able to detect single fluorophores (attached to a biomolecule of interest), the label density of the here-observed *Stm* is too high to observe distinct molecules. However, separate puncta can be observed outside the bacterial perimeter, which may indicate single molecules or small clusters. As these puncta appear to be located outside the bacterial cell wall, they may represent either secreted proteins or bacterial degradation products, containing one or more Hpg moieties. However, no conclusions can be drawn about these puncta, due to the current level of non-specific fluorophore labeling (fluorescent spots that are not associated with any observable bacterial structure in the electron micrograph). Further optimization of the fluorophore attachment by ccHc could provide more information about the origin of these extra-bacterial fluorescent puncta. Alternatively, a BONCAT-proteomics approach could be used to identify potential Hpg-labeled proteins secreted by intracellular *Stm*.

4.3 Conclusion

BONCAT-STORM-CLEM allowed for the detection of wild type *Stm* within the ultrastructural context of the host phagocyte, with high sensitivity and high resolution. Although further optimization of the technique is needed to reduce non-specific fluorophore labeling, it represents a promising new approach to study intracellular bacterial pathogens with higher accuracy and sensitivity than any previous method.[18,51–53] This opens up the possibility of imaging pathogens for which previous BONCAT approaches were not efficient. The combination of STORM-CLEM with BONCAT, tRNA/tRNA synthetase mutants, or bio-orthogonal cell-wall labeling will be valuable in studying the *in vivo* lifecycle of these pathogens.[11–13] Application of this technique to other areas in which bioorthogonal chemistry has been transformative would also add an extra dimension of ultrastructure to these fields.[54,55]

4.4 Experimental

Safety statement

All biological experiments with *S. enterica* serovar Typhimurium described in this study were performed under strict Bio Safety Level 2 conditions. Following fixation and disinfection of the tubes, further sample preparation for CLEM was performed under normal laboratory conditions. No unexpected or unusually high safety hazards were encountered.

Reagents

Lysogeny broth (LB) medium, methionine (Met), Dulbecco's modified Eagle medium (DMEM), Iscove's Modified Dulbecco's Medium (IMDM), GlutaMAX, pyruvate, 4-(2-hydroxyethyl)-1-piperazineethanesulfonic acid (HEPES), glycine, gelatin type A bloom 300 (gelatin), paraformaldehyde (PFA), bovine serum albumin (BSA), Copper(II) sulfate pentahydrate, (+)-sodium L-ascorbate, tris(3-hydroxypropyltriazolylmethyl)amine (THPTA), aminoguanidine hydrochloride, and IGEPAL CA-630 were purchased from Sigma-Aldrich, Zwijndrecht, The Netherlands. Non-essential amino acids (NEAA), 2-mercaptoethanol, L-glutamine, Hoechst 33342, 4',6-Diamidino-2-Phenylindole (DAPI) and azide-/alkyne-modified Alexa Fluor dyes (AF488 and AF647) were purchased from Thermo Fisher Scientific, Bleiswijk, The Netherlands. SelenoMet minimal medium was purchased from Molecular Dimensions, Sheffield, UK. D-propargylglycine (alkDala) was purchased from Combi-Blocks, San Diego, USA. EM-grade 8% paraformaldehyde and EM-grade 8% glutaraldehyde were purchased from Electron Microscopy Sciences, Hatfield, USA. Fetal calf serum (FCS) was purchased from VWR International, Amsterdam, The Netherlands. Penicillin G sodium and streptomycin sulphate were purchased from Duchefa, Haarlem, The Netherlands. Granulocyte-Macrophage Colony-Stimulating Factor (GM-CSF) was purchased from ImmunoTools, Friesoythe, Germany.

Organic synthesis

Synthesis of (S)-2-amino-4-azidobutanoic acid (L-azidohomoalanine; Aha)

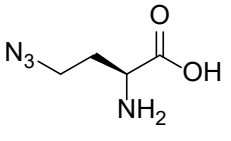

Aha was synthesized according to a previously described procedure by Zhang et al., 2010[56].

^{1}H-NMR (D_2O), 400 MHz: δ [ppm] = 4.05 (t, 1H, α-CH), 3.55 (t, 2H, γ-CH_2), 2.15 (m, 2H, β-CH_2).

Synthesis of (S)-2-Aminohex-5-ynoic acid (L-homopropargylglycine; Hpg)

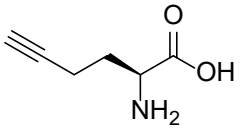

Hpg was synthesized according to previously described procedure by Li et al.[57], adjusted to obtain the enantiomerically pure L-Hpg variant based on Chenault et al.[58], Biagini et al.[59] and Dong et al.[60]

Chiral deprotection of *N*-acetyl-DL-homopropargylglycine (2-acetamidohex-5-ynoic acid)

A solution of 303 mg (1.13 mmol, 1 eq.) *N*-acetyl-DL-homopropargylglycine in 20 mL H_2O and adjusted to pH 7.5 using 1M NH_4OH. 1 mg kidney acylase I (≥2000 units/mg) was added and the mixture was stirred for 16 h at 37°C. The enzyme was recovered by centrifugation dialysis, using a 10kDa membrane at 4000 rpm for 35 min at 10°C. Next, the solution was acidified to pH 3 with 2M HCl and extracted with 3 x 20 mL diethyl ether. The organic layers were concentrated to retrieve the *N*-acetyl-D-homopropargylglycine. The aqueous layer was loaded on a pre-washed and regenerated Dowex 50WX8 cation exchange resin (60 mL). The column was washed with 5 x bed volume of water, maintaining a pH of 5.5 at the exit and eluted with 200 mL 1.5M NH_4OH. Product was detected by TLC and the eluate was concentrated and lyophilized to yield chirally pure L-Hpg (68 mg, 0.535 mmol, 95%) as a white powder.

^{1}H NMR (400MHz, D_2O): δ [ppm] = 4.11 (t, J = 6.4 Hz, 1H), 2.42 – 2.36 (m, 2H), 2.36 (s, 1H), 2.19 – 2.10 (m, 1H), 2.07 – 1.98 (m, 1H); 13C NMR (101MHz, D2O): δ 82.28, 71.16, 52.05, 28.44, 14.16; HRMS (ESI): $C_6H_9NO_2$ $[M+H]^+$ 128.06, found 128.07; $[\alpha]_{20}^{D}$: +32.4 (c = 1, 1 M HCl); Ref [60]: +28 (c = 1, 1 M HCl).

Bacterial culture, metabolic labeling and viability assessment based on growth rate

Stm SL1344 expressing DsRed[61] were grown overnight at 37°C in LB medium. The following day cultures were diluted 1:33 and grown at 37°C to an OD_{600} between 0.3-0.5. Subsequently bacteria were collected and resuspended in SelenoMet medium and supplemented with either 0.04, 0.4 or 4 mM Aha, 0.04, 0.4 or 4 mM

Hpg, 5 mM alkDala + 4 mM Met, 5 mM alkDala + 4 mM Aha (dual) or 4 mM Met (control). After 30, 60 and 120 minutes OD_{600} were measured and bacteria were collected by centrifugation for SDS-PAGE, flow cytometry analysis and DC infection experiments. For outgrowth experiments after 120 minutes of label incorporation, bacteria were collected by centrifugation and resuspended in LB medium and incubated for another 120 minutes with intermittent sampling. Throughout culturing, the medium was supplemented with 100 µg/ml ampicillin.

Mammalian cell culture and infection with *Stm*

DC2.4 cells were cultured in IMDM, supplemented with 10% heat-inactivated FCS, 2 mM GlutaMAX, 10 mM HEPES pH 7.3, 1 mM pyruvate, penicillin 100 l.U./mL and streptomycin 50 µg/mL, 50 µM 2-Mercaptoethanol and 1X non-essential amino acids.

Mouse bone marrow-derived dendritic cells (BMDCs) were generated from B57BL/6 mice bone marrow essentially as described[62] with some modifications. Briefly, bone marrow was flushed from femurs and tibia and cells were cultured in IMDM supplemented with 8% heat-inactivated FCS, 2 mM L-glutamine, 20 µM 2-Mercaptoethanol, penicillin 100 l.U./mL and streptomycin 50 µg/mL in the presence of 20 ng/mL GM-CSF. Medium was replaced on day 3 and 7 of culture and the cells were used between days 10 and 13.

Stm expressing DsRed and cultured in the presence of 0.4 mM Hpg for 30 minutes were added to the DC2.4 cells or BMDCs in the above medium without antibiotics as suspensions in PBS at an MOI of 50. After 45 minutes of incubation unbound/non-internalized *Stm* were washed off (2x PBS) and medium was replaced for immediate analysis (t = 0) or further incubation for 1 or 3 hours. Subsequently cells were subjected to flow cytometry, confocal microscopy or Tokuyasu sample preparation for CLEM. Label persistence was determined by incubating bacteria in cell medium at 37°C, collecting samples simultaneously with the cells to obtain identical time points, which were then subjected to flow cytometry sample preparation.

Analysis of label incorporation by in-gel fluorescence

At the indicated time points *Stm* were collected lysed with lysis buffer (50 mM HEPES pH 7.3, 150 mM NaCl and 1% IGEPAL) and incubated at 4°C for 18 h. Subsequently protein concentrations were determined with a Qubit 2.0 fluorimeter (Life Technologies) after which 20 µg of the protein was incubated for 1 h with ccHc-cocktail (0.1 M HEPES pH 7.3, 1 mM $CuSO_4$, 10 mM sodium ascorbate, 1 mM THPTA

ligand, 10 mM amino-guanidine, 5 µM AF647-azide. Samples were then resuspended in 4x SDS Sample buffer (250 mM Tris HCl pH 6.8, 8% w/v SDS, 40% glycerol, 0.04% w/v bromophenol blue, 5% 2-mercaptoethanol) and incubated at 100°C for 5 minutes before subjecting to SDS-PAGE. Gels were then directly imaged with a Bio-Rad Universal Hood III for in-gel visualization of the fluorescent labelling. As a loading control gels were stained with Coomassie Brilliant Blue. PageRuler Plus Prestained Protein Ladder (Thermo Scientific) was used as a protein standard.

Analysis of label incorporation by flow cytometry

Hpg-labeled *Stm* were collected by centrifugation (3000 rcf) at the indicated time points. DC2.4 cells infected with Hpg-*Stm* were harvested with 0.25% trypsin supplemented with 0.5 mM EDTA and collected by centrifugation (300 rcf) at the indicated time points. Both *Stm* and DC2.4 cells were subjected to the same treatment, with the exception of a differential centrifugation speed and a 1:20 predilution made for the bacteria after fixation: Cells were washed with PBS and fixed in suspension in 4% PFA for 18 h at 4°C, then washed again with PBS and incubated for 20 minutes in staining buffer (100 mM HEPES pH 7.3, 150 mM NaCl, 3% BSA, 0.1% IGEPAL CA-630 and 1 µg/mL Hoechst 33342), then washed again with PBS and incubated for 1 h with click cocktail (0.1 M HEPES pH 7.3, 1 mM $CuSO_4$, 10 mM sodium ascorbate, 1 mM THPTA ligand, 10 mM amino-guanidine, 5 µM AF647-azide), then washed repeatedly (3x5 minutes each) with FACS buffer (PBS pH 7.4, 1% FCS, 1% BSA, 0.1% NaN_3 and 2 mM EDTA) and resuspended in FACS buffer for measurements. All measurements were performed with a Guava easyCyte 12HT Benchtop Flow Cytometer and analyzed with FlowJo V10 (FlowJo software).

Preparation of *Stm*-infected BMDC samples for CLEM

Samples were prepared for cryo-sectioning as described elsewhere.[63,64] Briefly, BMDCs infected with *Stm* were fixed for 24 h in freshly prepared 2% PFA in 0.1 M phosphate buffer. Fixed cells were embedded in 12% gelatin and cut with a razor blade into approx. 1 mm^3 cubes. The sample blocks were infiltrated in phosphate buffer containing 2.3 M sucrose for 3 h. Sucrose-infiltrated sample blocks were mounted on aluminum pins and plunged in liquid nitrogen. The frozen samples were stored under liquid nitrogen.

Ultrathin cell sections were obtained as described elsewhere.[63,64] Briefly, the frozen sample was mounted in a cryo-ultramicrotome (Leica). The sample was trimmed to yield a squared block with a front face of about 300 x 250 µm (Diatome trimming tool). Using a diamond knife (Diatome) and antistatic devise (Leica) a ribbon of 150 nm thick sections was produced that was retrieved from the cryo-chamber with a

droplet of 1.15 M sucrose containing 1% methylcellulose. Obtained sections were transferred to a Formvar/carbon-coated titanium TEM grid, additionally coated with blue 0.2 µm FluoSpheres (Thermo Fisher) as fiducial markers.

Sections were labelled as follows; thawed cryo-sections on an EM grid were left for 30 minutes on the surface of 2% gelatin in phosphate buffer at 37°C. Subsequently grids were incubated on drops of PBS/Glycine and PBS/Glycine containing 1% BSA. Grids were then incubated on top of the ccHc-cocktail (0.1 M HEPES pH 7.3, 1 mM $CuSO_4$, 10 mM sodium ascorbate, 1 mM THPTA ligand, 10 mM amino-guanidine, 5 µM AF647-azide) for 1 h and washed 6 times with PBS. In case of confocal microscopy the grids were blocked again with PBS containing 1% BSA. After washing with PBS the sections were then labelled with DAPI (2 µg/ml), and additionally washed with PBS and water.

Microscopy and correlation

The CLEM approach used was adapted from Vicidomini et al.[65] Grids containing the sample sections were washed with 50% glycerol and placed on glass slides (pre-cleaned with 100% ethanol). Grids were then covered with a small drop of 50% glycerol after which a coverslip was mounted over the grid. Coverslips were fixed using Scotch Pressure Sensitive Tape. Samples were imaged with a Leica TCS SP8 confocal microscope (63x oil lens, N.A.=1.4). Confocal microscopy was used as it allowed to make image stacks from the sections at different focus planes, this was convenient as the sections were found to be in different focus planes whilst placed between the glass slides and coverslip.

In case of STORM imaging grids containing the sample sections were washed with GLOX buffer (100 µl PBS, 20 µl 50% glucose, 20 µl MEA 1M (ethanolamine) and 2µl GLOX (0.7 mg/ml GLOX, 5 mg/ml catalase in PBS) supplemented with 30% glycerol (60 µL) and placed on glass slides. Grids were then covered with a small drop of GLOX buffer after which a coverslip was mounted over the grid. STORM images were acquired using a Nikon N-STORM system configured for total internal reflection fluorescence (TIRF) imaging. Excitation inclination was tuned to adjust focus and to maximize the signal-to-noise ratio. AF647 was excited illuminating the sample with the 647 nm (160 mW, 1.9 kW cm^{-2}) laser line built into the microscope. Fluorescence was collected by means of a Nikon 100x, 1.4NA oil immersion objective and passed through a quad-band-pass dichroic filter (97335 Nikon). 20,000 frames at 50 Hz were acquired for the 647 channel. Images were recorded onto a 256 × 256 pixel region (pixel size 160 nm) of a CMOS camera. STORM images were analyzed with the STORM module of the NIS element Nikon software.[66]

After fluorescence or STORM microscopy the EM grid with the sections was removed from the glass slide, rinsed in distilled water and incubated for 5 minutes on droplets of uranyl acetate (0.4%)/methylcellulose (1.8%). Excess of uranyl acetate/methylcellulose was blotted away and grids were air-dried. EM imaging was performed with an Tecnai 12 BioTwin transmission electron microscope (FEI) at 120 kV acceleration voltage.[67]

Correlation of confocal and EM images was performed in Adobe Photoshop CS6. In Adobe Photoshop, the LM image was copied as a layer into the EM image and made 50% transparent. Transformation of the LM image was necessary to match it to the larger scale of the EM image. This was performed via isotropic scaling and rotation. Interpolation settings; bicubic smoother. Alignment at low magnification was carried out with the aid of nuclear DAPI staining in combination with the shape of the cells, at high magnification alignment was performed using the fiducial beads.[68]

STORM analysis

Resolution Calculations STORM module in the Nikon NIS-software is able to automatically calculate the localization precision distribution for each image. As it can be seen below, the maximum of the distribution is 20 nm, with most of the localizations below 20 and decreasing sharply from 20 to 25 nm.

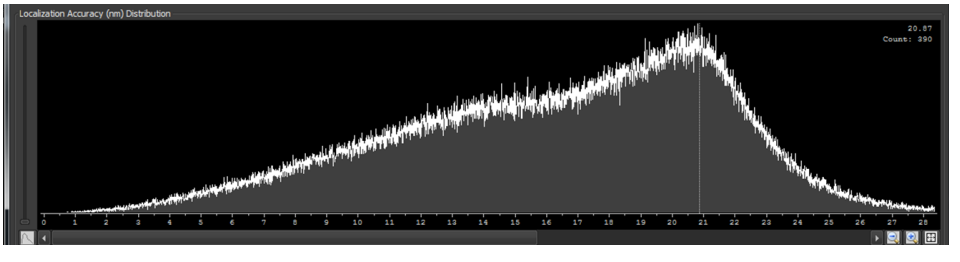

This numbers are well in agreement with the theoretical localization precision. The localization precision is defined as:

$$\sigma^2 = \frac{s^2 + a^2/12}{N} + \frac{8\pi^2 s^4 b^2}{a^2 N^2}$$

Where,
s: width of the PFS
N: number of detected photons
a: size of pixels on the camera
b: background intensity

Which can be simplified[69] to:

$$\sigma_x \geq \frac{s}{\sqrt{N}}$$

The average *s* for one of the images was calculated to be 338 ± 44 nm (for 538948 localizations). Also, the average for the number of photons for the same image is 1253, with a significant population above that value. Therefore, as the average s = 338 nm and the average N=1253 photons, $\sigma_x \geq 9.54\ nm$, resulting in the claimed 20 nm resolution. Single molecule localization and fitting was performed using the STORM module of NIS Elements by performing a Gaussian fitting based on the following parameters:

Minimum and maximum height: The darkest bright point was selected to be identified as a molecule and its brightness minus the background intensity was the minimum height. In our case it was set to 150. The maximum height for the used system with a sCMOS camera is 65000 and the baseline was set to 100.

For the PSF, the initial fit width was set to 300, with a minimum with of 200 and a maximum width of 400. The average for an image was calculated to be 338±44 nm (based on 538948 localizations).

This parameter was tested on different frames and optimized using all frames selected. The first 500 frames were discarded, due to incomplete photo-switching. This analysis yielded a molecule list in binary format from which multiple emitters are automatically discarded prior to analysis.

STORM NIS-software renders a molecule list in binary format whose coordinates are translated into an image. STORM images are shown in cross or Gaussian display mode in Nikon software. Cross takes into account directly the localizations while Gaussian, the one used in our case, is a Gaussian rendering of the localizations considering lateral localization accuracy (with an average of 17.9 ± 4.6) for each localization.

4.5 Supplemental Figures

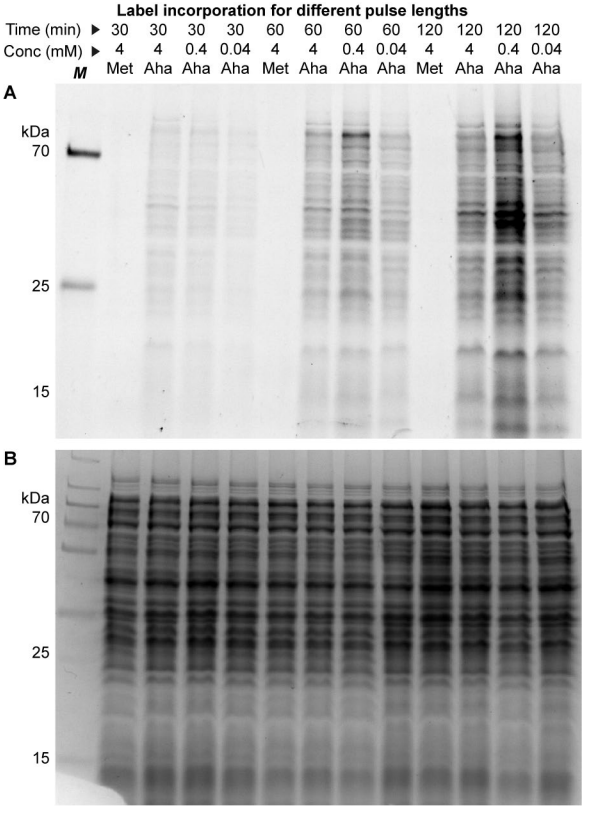

Figure S1. Optimization of Aha incorporation in Stm by SDS-PAGE. *Stm* were incubated with increasing concentrations of Aha or 4 mM Met (control) in SelenoMet medium for up to 120 min, then lysed, ccHc-reacted with AF647-alkyne and separated by SDS-PAGE for in-gel fluorescence analysis (**A**). Coomassie Brilliant Blue staining was used to show comparable protein loading for each lane (**B**).

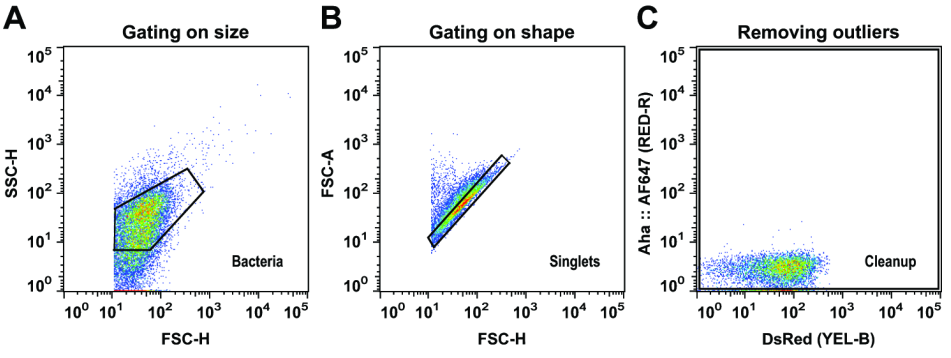

Figure S2. Gating strategy for measurement of *Stm* by flow cytometry. The bacteria were gated on size (**A**) and shape (**B**), and completely non-fluorescent were removed with a cleanup gate (**C**) to exclude any bacteria-unrelated particles from analysis.

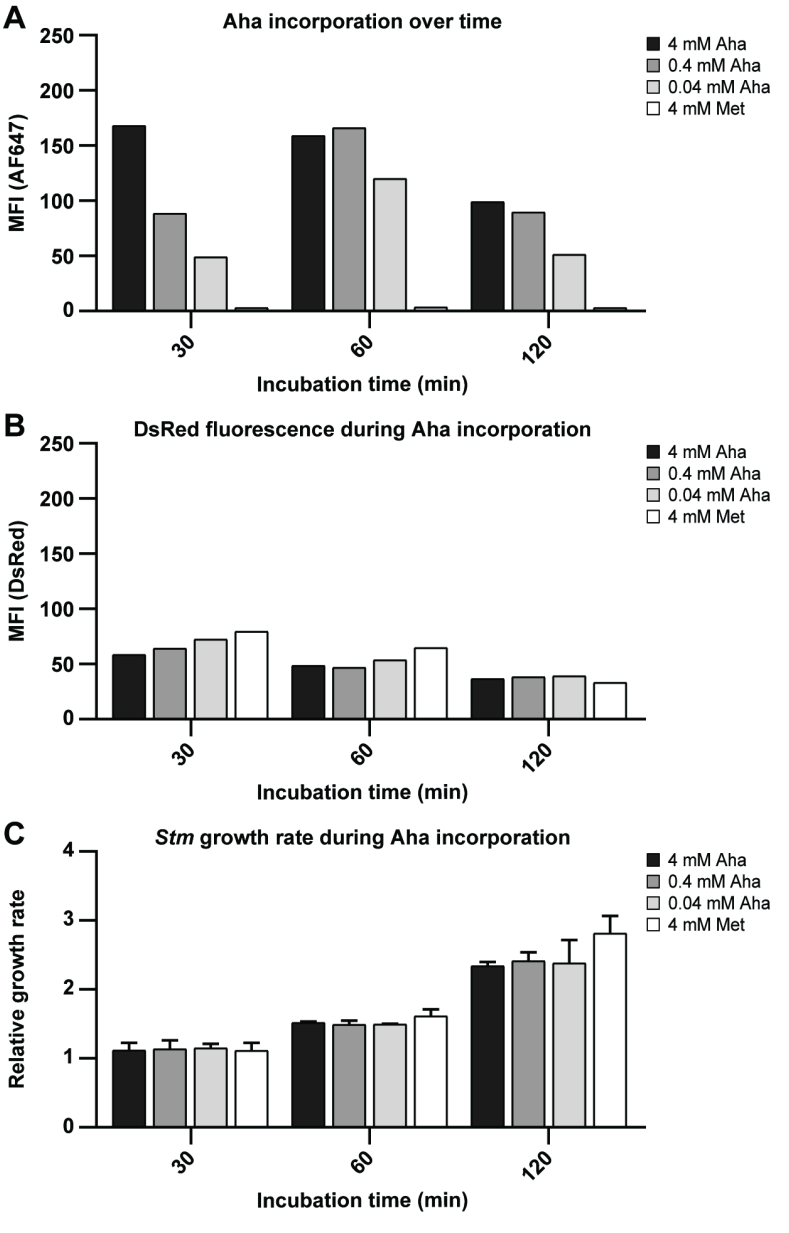

Figure S3. Optimization of Aha incorporation in *Stm* by flow cytometric analysis, part 2. DsRed-expressing *Stm* were incubated with increasing concentrations of Aha or 4 mM Met (control) in SelenoMet medium for up to 120 min, then ccHc-reacted with AF647-alkyne for detection by flow cytometry. (**A**) Aha incorporation over time is shown as the Mean Fluorescence Intensity (MFI) of the reacted AF647 (Figure 2A). (**B**) The effect of Aha incorporation on the DsRed fluorescent protein is shown as the MFI of DsRed (Figure 2B). (**C**) The effect of Aha incorporation on the viability of *Stm* is shown as the relative growth rate, determined by OD_{600} measurements, normalized to the initial OD value at t = 0. Error bars represent the standard deviation from the mean (n = 2).

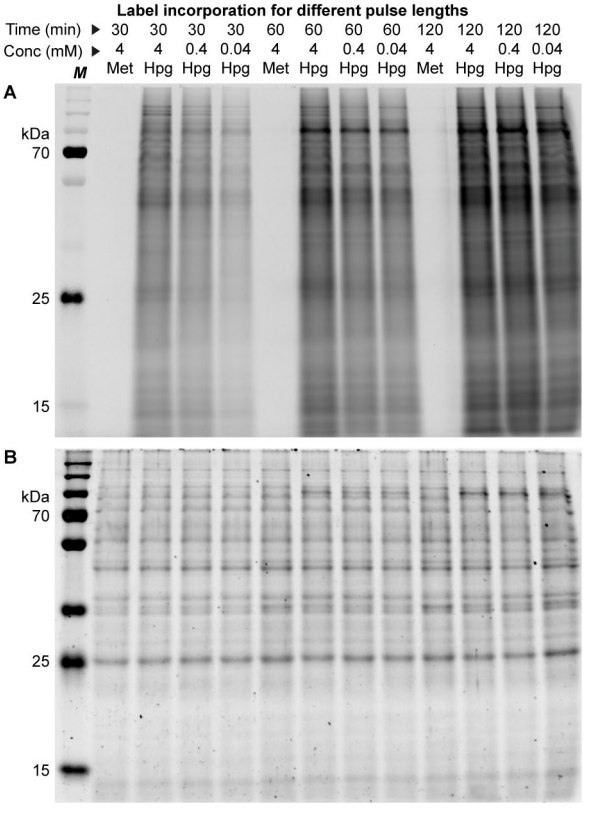

Figure S4. Optimization of Hpg incorporation in *Stm* by SDS-PAGE. *Stm* were incubated with increasing concentrations of Hpg or 4 mM Met (control) in SelenoMet medium for up to 120 min, then lysed, ccHc-reacted with AF647-azide and separated by SDS-PAGE for in-gel fluorescence analysis (**A**). Coomassie Brilliant Blue staining was used to show comparable protein loading for each lane (**B**).

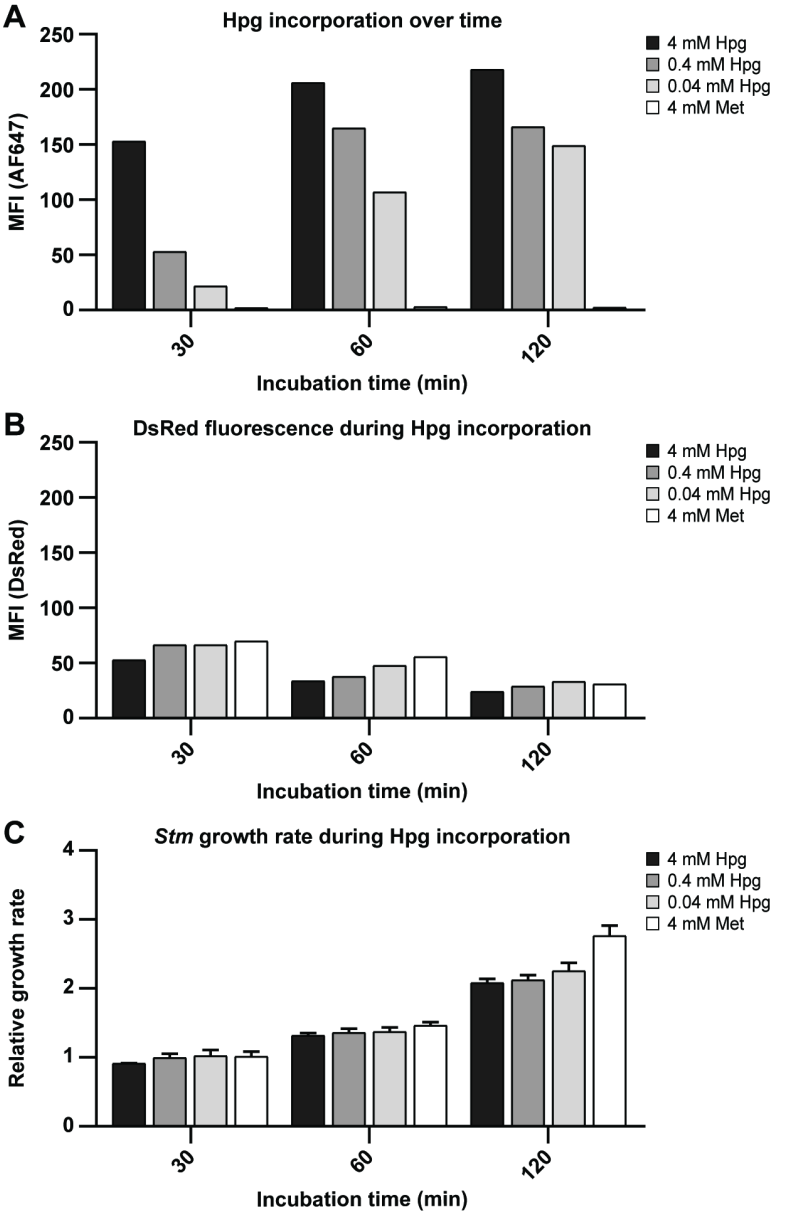

Figure S5. Optimization of Hpg incorporation in *Stm* by flow cytometric analysis, part 2. DsRed-expressing *Stm* were incubated with increasing concentrations of Hpg or 4 mM Met (control) in SelenoMet medium for up to 120 min, then ccHc-reacted with AF647-azide for detection by flow cytometry. (**A**) Hpg incorporation over time is shown as the Mean Fluorescence Intensity (MFI) of the reacted AF647 (Figure 3A). (**B**) The effect of Hpg incorporation on the DsRed fluorescent protein is shown as the MFI of DsRed (Figure 3B). (**C**) The effect of Hpg incorporation on the viability of *Stm* is shown as the relative growth rate, determined by OD_{600} measurements, normalized to the initial OD value at t = 0. Error bars represent the standard deviation from the mean (n = 2).

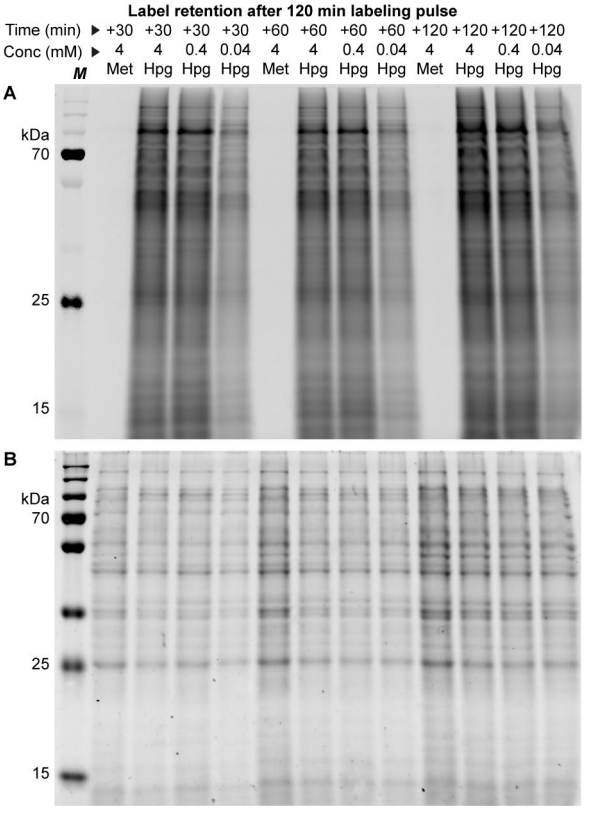

Figure S6. Hpg retention during outgrowth of *Stm* by SDS-PAGE. *Stm* were incubated with increasing concentrations of Hpg or 4 mM Met (control) in SelenoMet medium for up to 120 min, then washed and resuspended in fresh LB medium and additionally incubated for up to 120 min. *Stm* were then lysed, ccHc-reacted with AF647-azide and separated by SDS-PAGE for in-gel fluorescence analysis (**A**). Coomassie Brilliant Blue staining was used to show comparable protein loading for each lane (**B**).

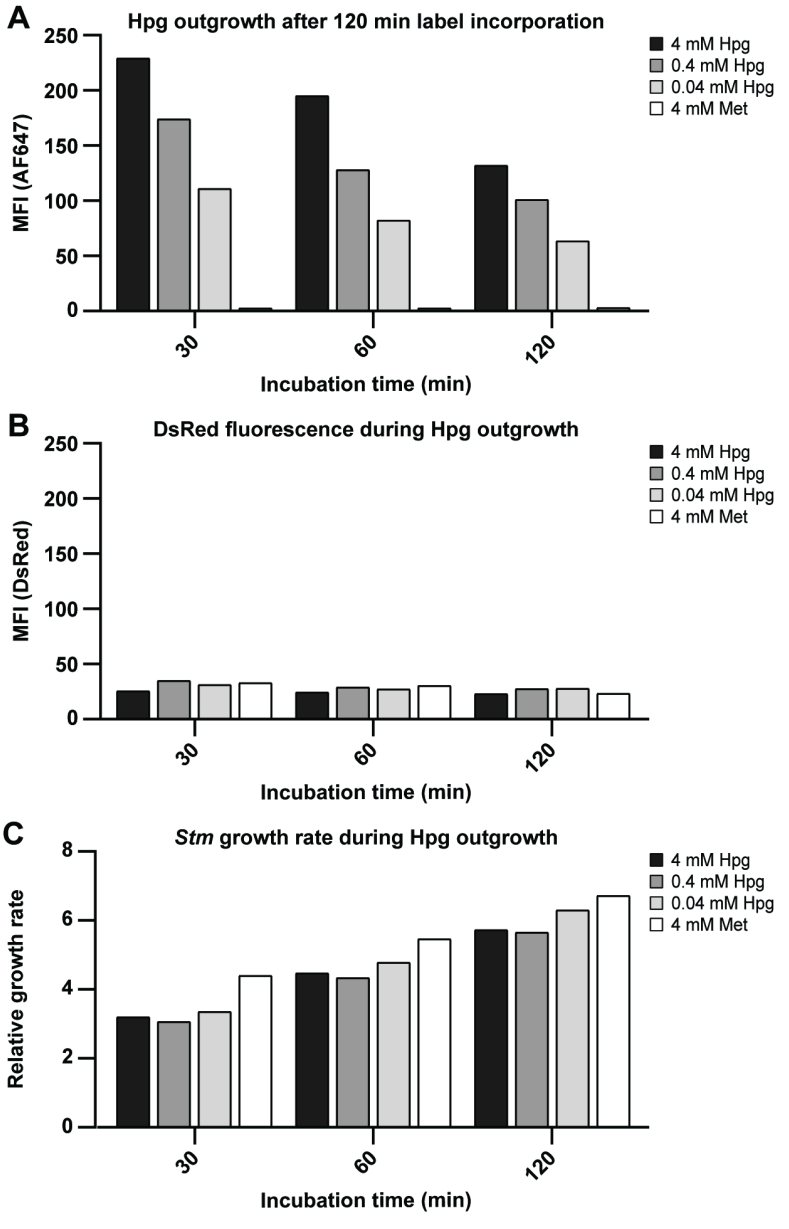

Figure S7. Label retention and growth recovery of Hpg-labeled *Stm* by flow cytometric analysis, part 2. DsRed-expressing *Stm* were incubated with increasing concentrations of Hpg or 4 mM Met (control) in SelenoMet medium for 120 min, washed with PBS and resuspended in fresh LB medium and incubated again for up to 120 min, then ccHc-reacted with AF647-azide for detection by flow cytometry. (**A**) Hpg retention over time (outgrowth) is shown as the Mean Fluorescence Intensity (MFI) of the reacted AF647 (Figure 4A). (**B**) The effect of Hpg outgrowth on the DsRed fluorescent protein is shown as the MFI of DsRed (Figure 4B). (**C**) The effect of Hpg incorporation on the growth recovery of *Stm* is shown as the relative growth rate, determined by OD_{600} measurements, normalized to the initial OD value at t = 0 before label incorporation (n = 1).

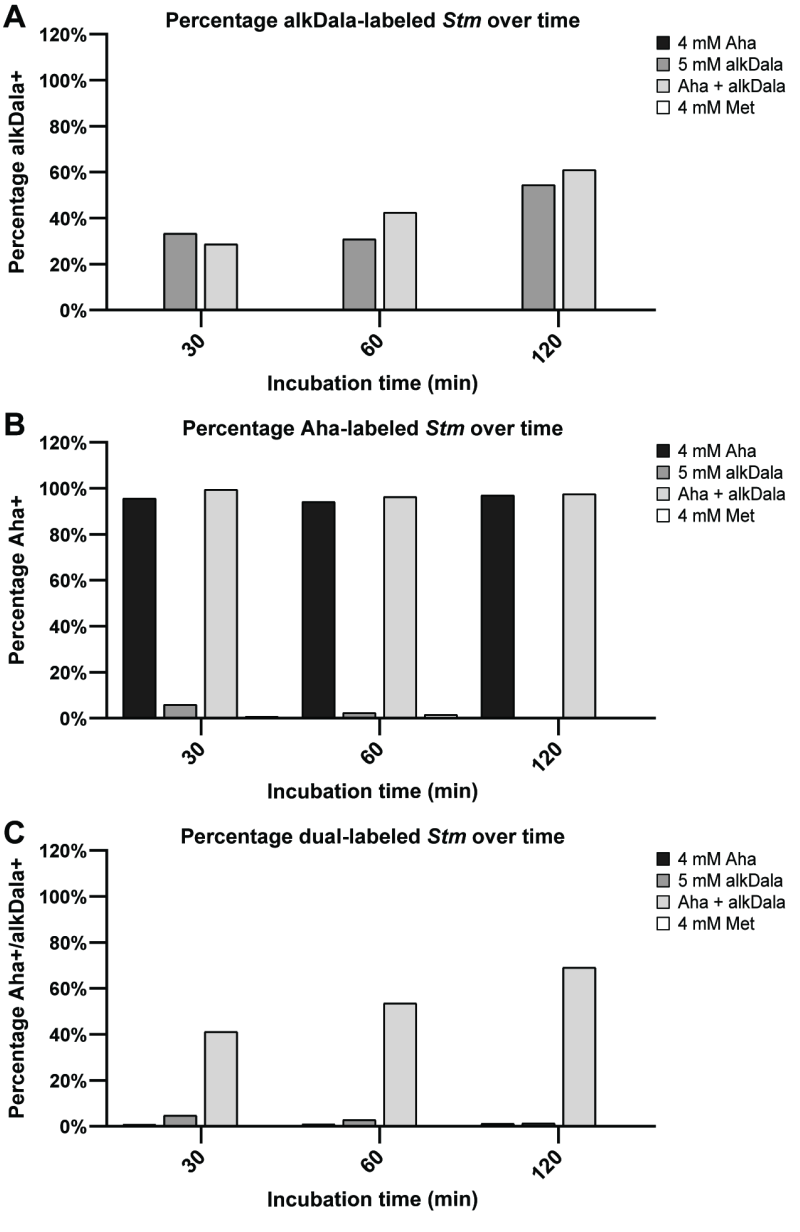

Figure S8. Optimization of alkDala labeling and Aha/alkDala dual labeling of *Stm* by flow cytometric analysis, part 2. *Stm* were incubated with 4 mM Aha, 4 mM Met + 5 mM alkDala, 4 mM Aha + 5 mM alkDala or 4 mM Met (control) in SelenoMet medium for up to 120 min, then ccHc-reacted with AF647-azide (alkDala) and AF488-alkyne (Aha) for detection by flow cytometry. (**A**) The percentage alkDala-labeled *Stm* (alkDala+) over time is shown, based on the fluorescence intensity of the reacted AF647 (Figure 5A). (**B**) The percentage Aha-labeled *Stm* (Aha+) over time is shown, based on the fluorescence intensity of the reacted AF488 (Figure 5B). (**C**) The percentage dual-labeled *Stm* (Aha+/alkDala+) over time is shown, based on the fluorescence intensity of the reacted AF647 and AF488 (Figure 5C).

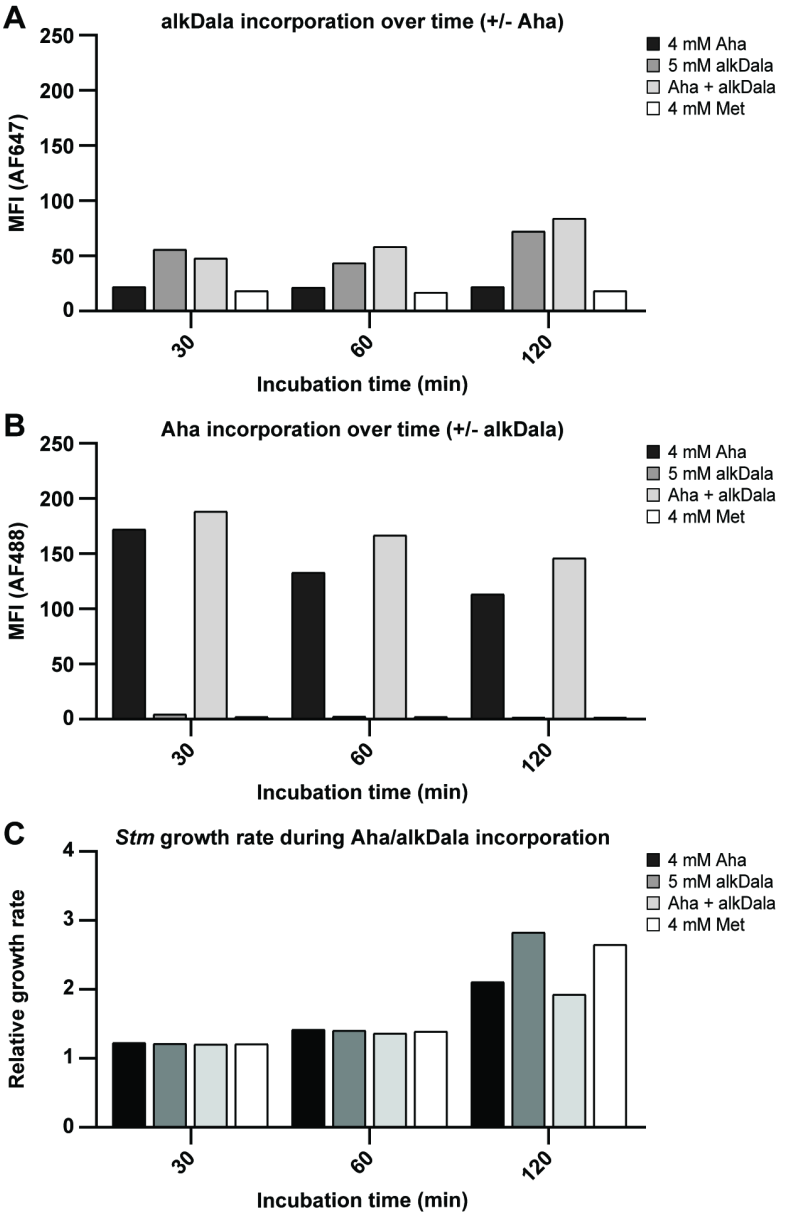

Figure S9. Optimization of alkDala labeling and Aha/alkDala dual labeling of *Stm* by flow cytometric analysis, part 3. *Stm* were incubated with 4 mM Aha, 4 mM Met + 5 mM alkDala, 4 mM Aha + 5 mM alkDala or 4 mM Met (control) in SelenoMet medium for up to 120 min, then ccHc-reacted with AF647-azide (alkDala) and AF488-alkyne (Aha) for detection by flow cytometry. (**A**) alkDala incorporation over time is shown as the Mean Fluorescence Intensity (MFI) of the reacted AF647 (Figure 5A). (**B**) Aha incorporation over time is shown as the MFI of the reacted AF488 (Figure 5B). (**C**) The effect of alkDala and/or Aha incorporation on the viability of *Stm* is shown as the relative growth rate, determined by OD_{600} measurements, normalized to the initial OD value at t = 0 (n = 1).

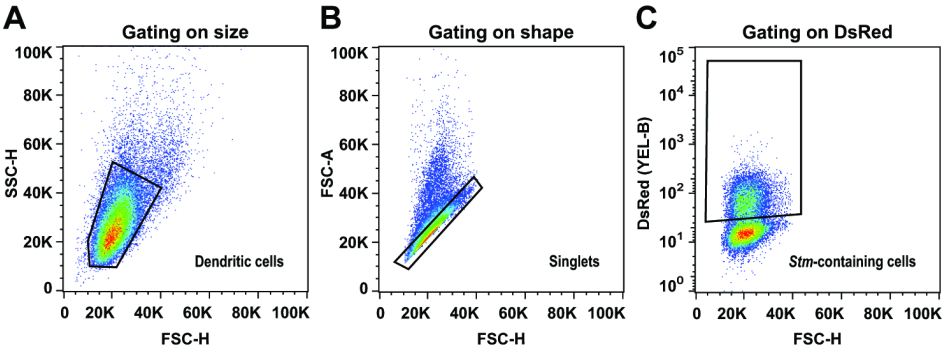

Figure S10. Gating strategy for measurement of *Stm*-containing DC2.4 cells by flow cytometry. DCs were gated on size (**A**) and shape (**B**) and *Stm*-containing cells were selected based on DsRed (**C**), which is only expressed by *Stm*.

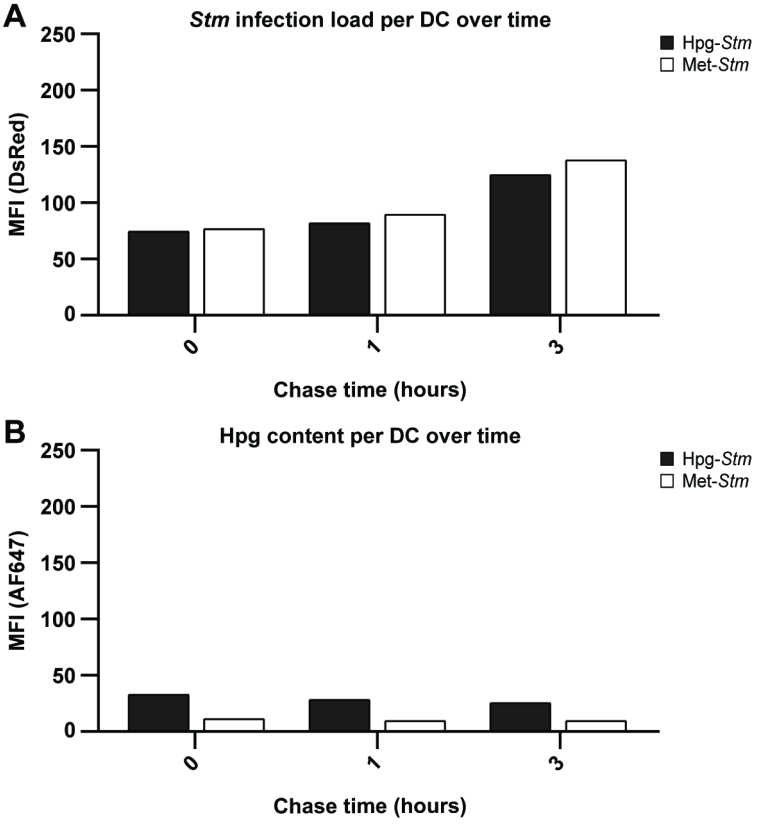

Figure S11. Infection controls, bioorthogonal label retention and *Stm* proliferation in DC2.4 cells, part 2. DsRed-expressing *Stm* were first incubated with 0.4 mM Hpg (Hpg-*Stm*) or 4 mM Met (Met-*Stm*) for 30 min in SelenoMet, then washed to remove excess Hpg and added to DCs at an MOI of 50 for 45 min (pulse). *Stm*-infected BDMCs were then washed to remove non-internalized *Stm* and incubated for an additional 0, 1 or 3 hours (chase), followed by ccHc-reaction with AF647-azide for detection by flow cytometry. (**A**) The *Stm* infection load was compared between Hpg-*Stm* and Met-*Stm* over time, based on the DsRed intensity per DC, shown as MFI. (**B**) The intracellular Hpg retention of *Stm* was followed over time in DCs, shown as MFI of the reacted AF647.

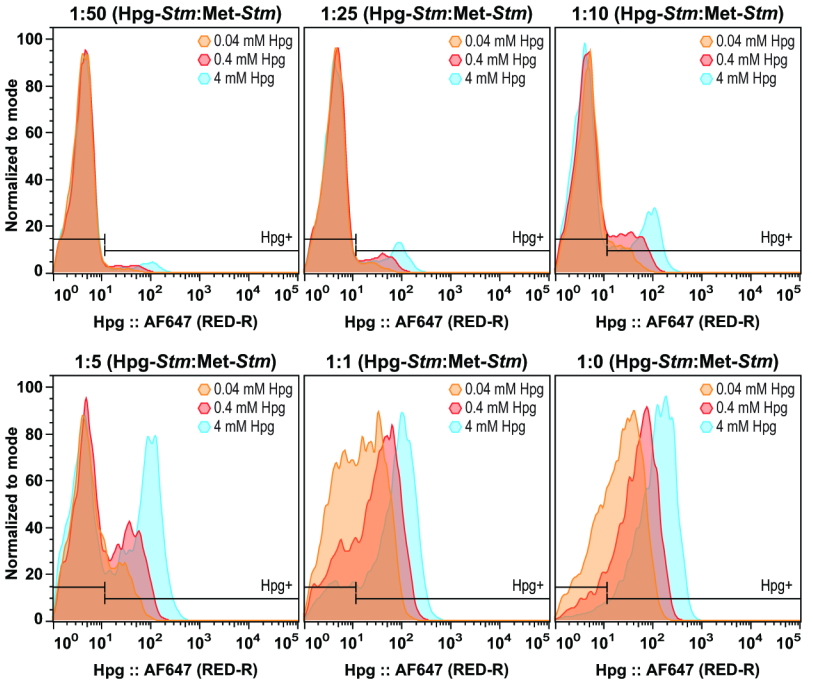

Figure S12. Hpg-labeled and unlabeled *Stm* mixed in various ratios for the optimization of STORM. Stm were grown in presence of increasing concentrations of Hpg (0.04-4 mM) and mixed in various ratios with unlabeled Stm, grown in presence of 4 mM Met.

4.6 References

(1) Mitchell, G.; Isberg, R. R. Innate Immunity to Intracellular Pathogens: Balancing Microbial Elimination and Inflammation. *Cell Host and Microbe*. Cell Press August 9, **2017**, pp 166–175.

(2) Pandey, S.; Kawai, T.; Akira, S. Microbial Sensing by Toll-like Receptors and Intracellular Nucleic Acid Sensors. *Cold Spring Harb. Perspect. Biol.* **2015**, *7* (1), a016246.

(3) Siegrist, M. S.; Whiteside, S.; Jewett, J. C.; Aditham, A.; Cava, F.; Bertozzi, C. R. D-Amino Acid Chemical Reporters Reveal Peptidoglycan Dynamics of an Intracellular Pathogen. *ACS Chem. Biol.* **2013**, *8* (3), 500–505.

(4) Shieh, P.; Siegrist, M. S.; Cullen, A. J.; Bertozzi, C. R. Imaging Bacterial Peptidoglycan with Near-Infrared Fluorogenic Azide Probes. *Proc. Natl. Acad. Sci.* **2014**, *111* (15), 5456–5461.

(5) Liechti, G. W.; Kuru, E.; Hall, E.; Kalinda, A.; Brun, Y. V.; Vannieuwenhze, M.; Maurelli, A. T. A New Metabolic Cell-Wall Labelling Method Reveals Peptidoglycan in Chlamydia Trachomatis. *Nature* **2014**, *506* (7489), 507–510.

(6) Swarts, B. M.; Holsclaw, C. M.; Jewett, J. C.; Alber, M.; Fox, D. M.; Siegrist, M. S.; Leary, J. A.; Kalscheuer, R.; Bertozzi, C. R. Probing the Mycobacterial Trehalome with Bioorthogonal Chemistry. *J. Am. Chem. Soc.* **2012**, *134* (39), 16123–16126.

(7) Backus, K. M.; Boshoff, H. I.; Barry, C. E. C. S.; Boutureira, O.; Patel, M. K.; D'Hooge, F.; Lee, S. S.; Via, L. E.; Tahlan, K.; Barry, C. E. C. S.; Davis, B. G. Uptake of Unnatural Trehalose Analogs as a Reporter for Mycobacterium Tuberculosis. *Nat. Chem. Biol.* **2011**, *7* (4), 228–235.

(8) Rodriguez-Rivera, F. P.; Zhou, X.; Theriot, J. A.; Bertozzi, C. R. Visualization of Mycobacterial Membrane Dynamics in Live Cells. *J. Am. Chem. Soc.* **2017**, *139* (9), 3488–3495.

(9) Dieterich, D. C.; Link, A. J.; Graumann, J.; Tirrell, D. A.; Schuman, E. M. Selective Identification of Newly Synthesized Proteins in Mammalian Cells Using Bioorthogonal Noncanonical Amino Acid Tagging (BONCAT). *Proc. Natl. Acad. Sci.* **2006**, *103* (25), 9482–9487.

(10) Mahdavi, A.; Szychowski, J.; Ngo, J. T.; Sweredoski, M. J.; Graham, R. L. J.; Hess, S.; Schneewind, O.; Mazmanian, S. K.; Tirrell, D. A. Identification of Secreted Bacterial Proteins by Noncanonical Amino Acid Tagging. *Proc. Natl. Acad. Sci.* **2014**, *111* (1), 433–438.

(11) Grammel, M.; Dossa, P. D.; Taylor-Salmon, E.; Hang, H. C. Cell-Selective Labeling of Bacterial Proteomes with an Orthogonal Phenylalanine Amino Acid Reporter. *Chem. Commun.* **2012**, *48* (10), 1473–1474.

(12) Grammel, M.; Zhang, M. M.; Hang, H. C. Orthogonal Alkynyl Amino Acid Reporter for Selective Labeling of Bacterial Proteomes during Infection. *Angew. Chemie - Int. Ed.* **2010**, *49* (34), 5970–5974.

(13) Lin, S.; Zhang, Z.; Xu, H.; Li, L.; Chen, S.; Li, J.; Hao, Z.; Chen, P. R. Site-Specific Incorporation of Photo-Cross-Linker and Bioorthogonal Amino Acids into Enteric Bacterial Pathogens. *J. Am. Chem. Soc.* **2011**, *133* (50), 20581–20587.

(14) Ngo, J. T.; Champion, J. A.; Mahdavi, A.; Tanrikulu, I. C.; Beatty, K. E.; Connor, R. E.; Yoo, T. H.; Dieterich, D. C.; Schuman, E. M.; Tirrell, D. A. Cell-Selective Metabolic Labeling of Proteins. *Nat. Chem. Biol.* **2009**, *5* (10), 715–717.

(15) Chande, A. G.; Siddiqui, Z.; Midha, M. K.; Sirohi, V.; Ravichandran, S.; Rao, K. V. S. Selective Enrichment of Mycobacterial Proteins from Infected Host Macrophages. *Sci. Rep.* **2015**, *5* (13430), 1–15.

(16) Hatzenpichler, R.; Connon, S. A.; Goudeau, D.; Malmstrom, R. R.; Woyke, T.; Orphan, V. J. Visualizing in Situ Translational Activity for Identifying and Sorting Slow-Growing

Archaeal - Bacterial Consortia. *Proc. Natl. Acad. Sci. U. S. A.* **2016**, *113* (28), E4069–E4078.

(17) van Elsland, D. M.; Bos, E.; Overkleeft, H. S.; Koster, A. J.; van Kasteren, S. I. The Potential of Bioorthogonal Chemistry for Correlative Light and Electron Microscopy: A Call to Arms. *J. Chem. Biol.* **2015**, *8* (4), 153–157.

(18) van Elsland, D. M.; Bos, E.; de Boer, W.; Overkleeft, H. S.; Koster, A. J.; van Kasteren, S. I. Detection of Bioorthogonal Groups by Correlative Light and Electron Microscopy Allows Imaging of Degraded Bacteria in Phagocytes. *Chem. Sci.* **2016**, *7* (1), 752–758.

(19) van Elsland, D. M.; Bos, E.; Pawlak, J. B.; Overkleeft, H. S.; Koster, A. J.; van Kasteren, S. I. Correlative Light and Electron Microscopy Reveals Discrepancy between Gold and Fluorescence Labelling. *J. Microsc.* **2017**, *267* (3), 309–317.

(20) Tornøe, C. W.; Christensen, C.; Meldal, M. Peptidotriazoles on Solid Phase: [1,2,3]-Triazoles by Regiospecific Copper(I)-Catalyzed 1,3-Dipolar Cycloadditions of Terminal Alkynes to Azides. *J. Org. Chem.* **2002**, *67* (9), 3057–3064.

(21) Rostovtsev, V. V.; Green, L. G.; Fokin, V. V.; Sharpless, K. B. A Stepwise Huisgen Cycloaddition Process: Copper(I)-Catalyzed Regioselective "Ligation" of Azides and Terminal Alkynes. *Angew. Chemie - Int. Ed.* **2002**, *41* (14), 2596–2599.

(22) Kiick, K. L.; Tirrell, D. A. Protein Engineering by in Vivo Incorporation of Non-Natural Amino Acids: Control of Incorporation of Methionine Analogues by Methionyl-TRNA Synthetase. *Tetrahedron* **2000**, *56* (48), 9487–9493.

(23) Abbe, E. Beiträge Zur Theorie Des Mikroskops Und Der Mikroskopischen Wahrnehmung: I. Die Construction von Mikroskopen Auf Grund Der Theorie. *Arch. für mikroskopische Anat.* **1873**, *9* (1), 413–418.

(24) Sahl, S. J.; Hell, S. W.; Jakobs, S. Fluorescence Nanoscopy in Cell Biology. *Nat. Rev. Mol. Cell Biol.* **2017**, *18* (11), 685–701.

(25) Beyond the Diffraction Limit. *Nature Photonics*. Nature Publishing Group July **2009**, p 361.

(26) Betzig, E.; Patterson, G. H.; Sougrat, R.; Lindwasser, O. W.; Olenych, S.; Bonifacino, J. S.; Davidson, M. W.; Lippincott-Schwartz, J.; Hess, H. F. Imaging Intracellular Fluorescent Proteins at Nanometer Resolution. *Science (80-.).* **2006**, *313* (5793), 1642–1645.

(27) Kopek, B. G.; Paez-Segala, M. G.; Shtengel, G.; Sochacki, K. A.; Sun, M. G.; Wang, Y.; Xu, C. S.; Van Engelenburg, S. B.; Taraska, J. W.; Looger, L. L.; Hess, H. F. Diverse Protocols for Correlative Super-Resolution Fluorescence Imaging and Electron Microscopy of Chemically Fixed Samples. *Nat. Protoc.* **2017**, *12* (5), 916–946.

(28) De Souza, N. Super-Resolution CLEM: Correlated Light and Electron Microscopy (CLEM) Is Particularly Powerful When Applied in Super-Resolution. *Nat. Methods* **2014**, *12* (1), 37.

(29) Suleiman, H.; Zhang, L.; Roth, R.; Heuser, J. E.; Miner, J. H.; Shaw, A. S.; Dani, A. Nanoscale Protein Architecture of the Kidney Glomerular Basement Membrane. *Elife* **2013**, *2013* (2).

(30) Watanabe, S.; Punge, A.; Hollopeter, G.; Willig, K. I.; Hobson, R. J.; Davis, M. W.; Hell, S. W.; Jorgensen, E. M. Protein Localization in Electron Micrographs Using Fluorescence Nanoscopy. *Nat. Methods* **2011**, *8* (1), 80–84.

(31) Sochacki, K. A.; Shtengel, G.; van Engelenburg, S. B.; Hess, H. F.; Taraska, J. W. Correlative Super-Resolution Fluorescence and Metal-Replica Transmission Electron Microscopy. *Nat. Methods* **2014**, *11* (3), 305–308.

(32) Watanabe, S.; Richards, J.; Hollopeter, G.; Hobson, R. J.; Davis, W. M.; Jorgensen, E. M. Nano-FEM: Protein Localization Using Photo-Activated Localization Microscopy and Electron Microscopy. *J. Vis. Exp.* **2012**, No. 69, 3995.

(33) Kopek, B. G.; Shtengel, G.; Xu, C. S.; Clayton, D. A.; Hess, H. F. Correlative 3D Superresolution Fluorescence and Electron Microscopy Reveal the Relationship of

Mitochondrial Nucleoids to Membranes. *Proc. Natl. Acad. Sci. U. S. A.* **2012**, *109* (16), 6136–6141.

(34) Kopek, B. G.; Shtengel, G.; Grimm, J. B.; Clayton, D. A.; Hess, H. F. Correlative Photoactivated Localization and Scanning Electron Microscopy. *PLoS One* **2013**, *8* (10), e77209.

(35) Tam, J.; Merino, D. Stochastic Optical Reconstruction Microscopy (STORM) in Comparison with Stimulated Emission Depletion (STED) and Other Imaging Methods. *J. Neurochem.* **2015**, *135* (4), 643–658.

(36) Godin, A. G.; Lounis, B.; Cognet, L. Super-Resolution Microscopy Approaches for Live Cell Imaging. *Biophys. J.* **2014**, *107* (8), 1777–1784.

(37) MacDonald, L.; Baldini, G.; Storrie, B. Does Super Resolution Fluorescence Microscopy Obsolete Previous Microscopic Approaches to Protein Co-Localization? *Methods Mol. Biol.* **2015**, *1270*, 255–275.

(38) Oddone, A.; Vilanova, I. V.; Tam, J.; Lakadamyali, M. Super-Resolution Imaging with Stochastic Single-Molecule Localization: Concepts, Technical Developments, and Biological Applications. *Microsc. Res. Tech.* **2014**, *77* (7), 502–509.

(39) Dempsey, G. T.; Vaughan, J. C.; Chen, K. H.; Bates, M.; Zhuang, X. Evaluation of Fluorophores for Optimal Performance in Localization-Based Super-Resolution Imaging. *Nat. Methods* **2011**, *8* (12), 1027–1040.

(40) Alpuche-Aranda, C. M.; Racoosin, E. L.; Swanson, J. A.; Miller, S. I. Salmonella Stimulate Macrophage Macropinocytosis and Persist within Spacious Phagosomes. *J. Exp. Med.* **1994**, *179* (2), 601–608.

(41) Haraga, A.; Ohlson, M. B.; Miller, S. I. Salmonellae Interplay with Host Cells. *Nature Reviews Microbiology*. Nature Publishing Group January **2008**, pp 53–66.

(42) Forest, C. G.; Ferraro, E.; Sabbagh, S. C.; Daigle, F. Intracellular Survival of Salmonella Enterica Serovar Typhi in Human Macrophages Is Independent of Salmonella Pathogenicity Island (SPI)-2. *Microbiology* **2010**, *156* (12), 3689–3698.

(43) Krieger, V.; Liebl, D.; Zhang, Y.; Rajashekar, R.; Chlanda, P.; Giesker, K.; Chikkaballi, D.; Hensel, M. Reorganization of the Endosomal System in Salmonella-Infected Cells: The Ultrastructure of Salmonella-Induced Tubular Compartments. *PLoS Pathog.* **2014**, *10* (9), e1004374.

(44) Scanu, T.; Spaapen, R. M.; Bakker, J. M.; Pratap, C. B.; Wu, L. en; Hofland, I.; Broeks, A.; Shukla, V. K.; Kumar, M.; Janssen, H.; Song, J. Y.; Neefjes-Borst, E. A.; te Riele, H.; Holden, D. W.; Nath, G.; Neefjes, J. Salmonella Manipulation of Host Signaling Pathways Provokes Cellular Transformation Associated with Gallbladder Carcinoma. *Cell Host Microbe* **2015**, *17* (6), 763–774.

(45) van Elsland, D. M. A Bioorthogonal Chemistry Approach to the Study of Biomolecules in Their Ultrastructural Cellular Context, **2018**.

(46) West, M. A.; Wallin, R. P. A.; Matthews, S. P.; Svensson, H. G.; Zaru, R.; Ljunggren, H. G.; Prescott, A. R.; Watts, C. Enhanced Dendritic Cell Antigen Capture via Toll-like Receptor-Induced Actin Remodeling. *Science (80-.).* **2004**, *305* (5687), 1153–1157.

(47) Méresse, S.; Steele-Mortimer, O.; Finlay, B. B.; Gorvel, J. P. The Rab7 GTPase Controls the Maturation of Salmonella Typhimurium-Containing Vacuoles in HeLa Cells. *EMBO J.* **1999**, *18* (16), 4394–4403.

(48) Bakkum, T.; van Leeuwen, T.; Sarris, A. J. C.; van Elsland, D. M.; Poulcharidis, D.; Overkleeft, H. S.; van Kasteren, S. I. Quantification of Bioorthogonal Stability in Immune Phagocytes Using Flow Cytometry Reveals Rapid Degradation of Strained Alkynes. *ACS Chem. Biol.* **2018**, *13* (5), 1173–1179.

(49) Lowrie, D. B.; Aber, V. R.; Carrol, M. E. Division and Death Rates of Salmonella Typhimurium inside Macrophages: Use of Penicillin as a Probe. *J. Gen. Microbiol.* **1979**, *110* (2), 409–419.

(50) Nahidiazar, L.; Agronskaia, A. V.; Broertjes, J.; van den Broek, B.; Jalink, K. Optimizing Imaging Conditions for Demanding Multi-Color Super Resolution Localization Microscopy. *PLoS One* **2016**, *11* (7), e0158884.

(51) Ngo, J. T.; Adams, S. R.; Deerinck, T. J.; Boassa, D.; Rodriguez-Rivera, F.; Palida, S. F.; Bertozzi, C. R.; Ellisman, M. H.; Tsien, R. Y. Click-EM for Imaging Metabolically Tagged Nonprotein Biomolecules. *Nat. Chem. Biol.* **2016**, *12* (6), 459–465.

(52) Scotuzzi, M.; Kuipers, J.; Wensveen, D. I.; De Boer, P.; Hagen, K. C. W.; Hoogenboom, J. P.; Giepmans, B. N. G. Multi-Color Electron Microscopy by Element-Guided Identification of Cells, Organelles and Molecules. *Sci. Rep.* **2017**, *7* (March), 1–8.

(53) Adams, S. R.; Mackey, M. R.; Ramachandra, R.; Palida Lemieux, S. F.; Steinbach, P.; Bushong, E. A.; Butko, M. T.; Giepmans, B. N. G.; Ellisman, M. H.; Tsien, R. Y. Multicolor Electron Microscopy for Simultaneous Visualization of Multiple Molecular Species. *Cell Chem. Biol.* **2016**, *23* (11), 1417–1427.

(54) Mateos-Gil, P.; Letschert, S.; Doose, S.; Sauer, M. Super-Resolution Imaging of Plasma Membrane Proteins with Click Chemistry. *Front. Cell Dev. Biol.* **2016**, *4* (SEP), 1–16.

(55) Erdmann, R. S.; Takakura, H.; Thompson, A. D.; Rivera-Molina, F.; Allgeyer, E. S.; Bewersdorf, J.; Toomre, D.; Schepartz, A. Super-Resolution Imaging of the Golgi in Live Cells with a Bioorthogonal Ceramide Probe. *Angew. Chemie - Int. Ed.* **2014**, *53* (38), 10242–10246.

(56) Zhang, M. M.; Tsou, L. K.; Charron, G.; Raghavan, A. S.; Hang, H. C. Tandem Fluorescence Imaging of Dynamic S-Acylation and Protein Turnover. *Proc. Natl. Acad. Sci. U. S. A.* **2010**, *107* (19), 8627–8632.

(57) Li, N.; Lim, R. K. V; Edwardraja, S.; Lin, Q. Copper-Free Sonogashira Cross-Coupling for Functionalization of Alkyne-Encoded Proteins in Aqueous Medium and in Bacterial Cells. *J. Am. Chem. Soc.* **2011**, *133* (39), 15316–15319.

(58) Chenault, H. K.; Dahmer, J.; Whitesides, G. M. Kinetic Resolution of Unnatural and Rarely Occurring Amino Acids: Enantioselective Hydrolysis of N-Acyl Amino Acids Catalyzed by Acylase I. *J. Am. Chem. Soc.* **1989**, *111* (16), 6354–6364.

(59) Biagini, S. C. G.; Gibson, S. E.; Keen, S. P. Cross-Metathesis of Unsaturated Alpha-Amino Acid Derivatives. *J. Chem. Soc. Perkin Trans. 1* **1998**, *1*, 2485–2500.

(60) Dong, S.; Merkel, L.; Moroder, L.; Budisa, N. Convenient Syntheses of Homopropargylglycine. *J. Pept. Sci.* **2008**, *14* (10), 1148–1150.

(61) Albers, H. M. H. G.; Kuijl, C.; Bakker, J.; Hendrickx, L.; Wekker, S.; Farhou, N.; Liu, N.; Blasco-Moreno, B.; Scanu, T.; Den Hertog, J.; Celie, P.; Ovaa, H.; Neefjes, J. Integrating Chemical and Genetic Silencing Strategies to Identify Host Kinase-Phosphatase Inhibitor Networks That Control Bacterial Infection. *ACS Chem. Biol.* **2014**, *9* (2), 414–422.

(62) Lutz, M. B.; Kukutsch, N.; Ogilvie, A. L. .; Rößner, S.; Koch, F.; Romani, N.; Schuler, G. An Advanced Culture Method for Generating Large Quantities of Highly Pure Dendritic Cells from Mouse Bone Marrow. *J. Immunol. Methods* **1999**, *223* (1), 77–92.

(63) Peters, P. J. Cryo-Immunogold Electron Microscopy. *Curr. Protoc. Cell Biol.* **1999**, *2* (1), 4.7.1-4.7.12.

(64) Peters, P. J.; Bos, E.; Griekspoor, A. Cryo-Immunogold Electron Microscopy. *Curr. Protoc. Cell Biol.* **2006**, *30* (1), 4.7.1-4.7.19.

(65) Vicidomini, G.; Gagliani, M. C.; Cortese, K.; Krieger, J.; Buescher, P.; Bianchini, P.; Boccacci, P.; Tacchetti, C.; Diaspro, A. A Novel Approach for Correlative Light Electron Microscopy Analysis. *Microsc. Res. Tech.* **2010**, *73* (3), 215–224.

(66) Van Der Zwaag, D.; Vanparijs, N.; Wijnands, S.; De Rycke, R.; De Geest, B. G.; Albertazzi, L. Super Resolution Imaging of Nanoparticles Cellular Uptake and Trafficking. *ACS Appl. Mater. Interfaces* **2016**, *8* (10), 6391–6399.

(67) Kremer, J. R.; Mastronarde, D. N.; McIntosh, J. R. Computer Visualization of Three-

Dimensional Image Data Using IMOD. *J. Struct. Biol.* **1996**, *116* (1), 71–76.
(68) Kukulski, W.; Schorb, M.; Welsch, S.; Picco, A.; Kaksonen, M.; Briggs, J. A. G. Correlated Fluorescence and 3D Electron Microscopy with High Sensitivity and Spatial Precision. *J. Cell Biol.* **2011**, *192* (1), 111–119.
(69) Deschout, H.; Zanacchi, F. C.; Mlodzianoski, M.; Diaspro, A.; Bewersdorf, J.; Hess, S. T.; Braeckmans, K. Precisely and Accurately Localizing Single Emitters in Fluorescence Microscopy. *Nat. Methods* **2014**, *11* (3), 253–266.